Future projections in tropical cyclone activity over multiple CORDEX domains from RegCM4 CORDEX-CORE simulations

Article

Accepted Version

Future projections in tropical cyclone activity over multiple CORDEX domains from RegCM4 CORDEX-CORE simulations

José Abraham Torres-Alavez[1], Russell Glazer[1], Filippo Giorgi[1], Erika Coppola[1], Xuejie Gao[2], Kevin I. Hodges[3], Sushant Das[1], Moetasim Ashfaq[4], Marco Reale[1,5] and Taleena Sines[1]

1) Earth System Physics, The Abdus Salam International Centre for Theoretical Physics (ICTP), Trieste, Italy
2) Climate Change Research Center, Institute of Atmospheric Physics, Chinese Academy of Sciences, Beijing, China
3) Department of Meteorology, University of Reading, Reading, United Kingdom
4) Computer Science and Engineering Division, Oak Ridge National Laboratory, Oak Ridge, TN, USA
5) Istituto di Oceanografia e di Geofisica Sperimentale (OGS), Trieste, Italy

Submitted
to

Climate Dynamics

July 2020

Corresponding Author: José Abraham Torres Alavez (email: jtorres@ictp.it), Earth System Physics Section, The Abdus Salam International Centre for Theoretical Physics (ICTP), Trieste, Italy. https://orcid.org/0000-0002-3704-5822.

Abstract

The characteristics of tropical cyclone (TC) activity over 5 TC basins lying within four Coordinated Regional Downscaling Experiment (CORDEX) domains are examined for present and future climate conditions using a new ensemble of projections completed as part of the CORDEX-CORE initiative with the regional climate model RegCM4. The simulations are conducted on a 25 km horizontal grid spacing using lateral and lower boundary forcing from three CMIP5 general circulation models (GCMs) under two Representative Concentration Pathways (RCP2.6 and RCP8.5). The RegCM4 is capable of capturing most features of the observed TC climatology over the different basins and exhibits a improved simulation of several TC statistics compared to the driving GCMs, except over the North Indian Ocean basin. Analysis of the influence of global warming on TC activity indicates significant increases in their frequency over the North Indian Ocean, the Northwest Pacific and Eastern Pacific regions. These changes are consistent with an increase in mid-tropospheric relative humidity. On the other hand, the North Atlantic and Australasia regions show a decrease in TC frequency, mostly associated with an increase in wind shear. We also find a predominant increase in the frequency of the most intense TCs over most domains. Our study shows robust and statistically significant responses often, but not always, in line with previous studies, still implying the presence of significant uncertainties. A robust assessment of TC changes requires analyses of ensembles of simulations with high-resolution models capable of representing the response of different TC characteristics to key atmospheric factors.

Keywords: Regional climate model, CORDEX-CORE, Tropical cyclones, Climate change.

1. Introduction

Tropical cyclones (TCs) have a wide-ranging socioeconomic impact (Camargo and Wing 2016; Knutson et al. 2019), mostly related to the destructive effects of their intense winds, storm surges, and extreme precipitation. They also play a beneficial role in providing freshwater for agriculture and other water resources (Czajkowski et al. 2013; Rappaport 2000; Dominguez and Magaña 2018). Therefore, increasing our knowledge of how TC characteristics could change with anthropogenic warming is critical to assessing their impacts on human and natural systems and to developing suitable adaptation and mitigation strategies.

Recently, numerous studies have examined how TC genesis, occurrence, maximum wind speed and mean precipitation could change under warmer conditions. These have used General Circulation Models (GCMs; Bengtsson et al., 2007; Camargo 2013; Murakami et al. 2012a, b, 2014; Knutson et al. 2015; Sugi et al. 2017; Bacmeister et al. 2018; Wehner et al. 2018) and regional climate models (RCMs), with a focus on different ocean basins (Lavender and Walsh 2011; Knutson et al. 2013; Diro et al. 2014; Manganello et al. 2014; Jin et al. 2016; Wang et al. 2017). These studies have shown a wide range of basin-dependent potential shifts in future TC characteristics with respect to TC frequency of occurrence and the frequency of very intense TCs (Category 4–5). For both these variables, for example, there is no consistent signal of change across individual basins (Camargo et al. 2013; Knutson et al. 2020*)*, which might be related to differences in model resolution, physics, dynamical core or sea-surface temperatures (SSTs) warming patterns (e.g. Li et al. 2010; Walsh et al. 2010; Murakami et al. 2012b; Martínez-Sanchez and Cavazos 2014; Reed et al. 2015; Fuentes-Franco et al. 2017; Hsu et al. 2019).

The World Meteorological Organization (WMO) task team report (Knutson et al. 2010), the Fifth Assessment Report (AR5) of the Intergovernmental Panel on Climate Change (IPCC; Christensen et al. 2013), and Walsh et al. (2016) summarized the results of many modeling studies of future changes in TC climatology. They concluded that increasing greenhouse gas (GHG) concentrations is projected to lead to a global decrease in TC frequency by 5-30%, but with an increase in the frequency of TC categories 4 and 5 by up to 25%. They also reported an increase in TC lifetime and maximum intensity, along with increases in TC rainfall rate by 5–20%. However, these conclusions are highly basin- and scenario-dependent, and many uncertain aspects remain, such as the patterns of decrease in TC frequency, increase in very intense TCs (Category 4–5), and slowdown in TC translation speed (Knutson et al. 2020).

There is thus a need for further investigation of the TC's response to global warming, especially at the regional scale. This is particularly important in view of the fact that current GCMs used in the Coupled Model Intercomparison Project (CMIP) still suffer from the lack of sufficient model resolution to resolve important TC processes. One way to approach this issue is to use higher resolution RCMs (Murakami et al. 2012b; Giorgi 2019), which have demonstrated a relatively good performance in reproducing the general characteristics of TCs and have been used to assess the response of TC characteristics to global warming in different basins (e.g. Lavender and Walsh 2011; Knutson et al. 2013; Diro et al. 2014; Fuentes-Franco et al. 2017; Wang et al. 2017; Vishnu et al. 2019).

In this regard, recently a new set of 21st century projections with the RegCM4 regional model (Giorgi et al. 2012) have been completed for multiple domains defined by the COordinated Regional Downscaling EXperiment (CORDEX, Giorgi et al. 2009) as part of the CORDEX-CORE initiative (Gutowski et al. 2016). The simulations are conducted with 25 km

grid spacing through downscaling of three GCMs from the CMIP5 ensemble (Taylor et al. 2012) for two GHG Representative Concentration Pathways (RCPs), the low end RCP2.6 and high end RCP8.5 (Moss et al. 2008). The availability of this new dataset thus offers the opportunity to analyze TC characteristics over multiple basins and their response to different global warming scenarios within a common simulation framework. The unique aspect of this analysis is that the different basins and scenarios are treated in a fully consistent way from a set of high-resolution RCM experiments following the same simulation protocol, which facilitates cross-basin and cross-scenario intercomparisons. In fact, previous RCM-based work mostly focused on individual basins and/or scenarios.

We analyze a range of TC characteristics, such as frequency of occurrence, intensity, duration, track position, frequency of high intensity TCs, and precipitation associated with TCs. In addition, we analyze both the model performance in reproducing these characteristics under present day climate conditions, and the changes induced by global climate warming scenarios. In particular, we attempt to identify the physical mechanisms driving the simulated TC responses and discuss relevant underlying uncertainties.

The paper is organized as follows. The data, TC tracking algorithm and methods are first described in section 2. Then, the evaluation of the model performance is presented in section 3, while section 4 and 5 examine the changes in tropical cyclone climatology and their driving mechanisms for the mid- (2041–2060) and late 21st century (2075–2099), under the RCP2.6 and RCP8.5 radiative forcing scenarios. A summary of the results, with final considerations, are finally given in section 6.

2. Data and methods

a. Regional Climate Model

Here we analyze simulations with the RegCM version 4, or RegCM4, the latest version of the RCM developed by the Abdus Salam International Centre for Theoretical Physics (ICTP; Giorgi et al. 2012). RegCM4 utilizes the hydrostatic dynamical core from the mesoscale model MM5 (Grell et al. 1994), with split-explicit advection, sigma-p vertical coordinates and an Arakawa-b staggered horizontal grid. The model includes multiple physics options, and for each region, physics parameterizations were selected based on a series of preliminary experiments using boundary conditions from reanalyses aimed at optimizing the model performance over the different domains. This selection was not done specifically with the aim of TC simulation but for the CORDEX-CORE application as a whole and, as a standard procedure before use of RegCM4 for production runs, was based on standard metrics such as biases and probability density functions of variables such as temperature, precipitation and winds. For the Central America domain Diro et al. (2014) and Fuentes-Franco et al. (2017) have shown that the RegCM4 simulation of TC characteristics such as track density, frequency, lifetime and intensity is sensitive to the convection scheme and ocean flux parametrization used, and these studies have contributed to our choice of optimal physics schemes for this domain. The scheme utilized for each domain are reported in Table 1.

The RegCM4 simulations follow the CORDEX-CORE protocol (Giorgi et al. 2012, Giorgi and Gutowsky 2015, Gutowski et al. 2016) over nine CORDEX domains (Giorgi et al. 2009). They extend from 1970 to 2099 with a horizontal grid spacing of 25 km and 23 vertical sigma levels. Three GCMs are downscaled for each of two RCPs, the low level RCP2.6 and the high-end RCP8.5 (Moss et al. 2008). Table 1 reports the driving GCMs used for each RegCM4 simulation (for the Northwest Pacific region only two simulations are currently available). These

GCMs were chosen within the CORDEX-CORE protocol as performing generally well over the domains of interest (Elguindi et al. 2014) and having a low-, medium-, and high-equilibrium climate sensitivity (ECS), so as to approximately cover the CMIP5 climate sensitivity range.

The GCMs provide 6-hourly driving wind, pressure, temperature and water vapor as lateral boundary conditions for the RegCM4, and daily Sea Surface Temperature (SST) as lower boundary condition. In addition, the GHG concentrations in the RegCM4 are updated every 10 years based on observations for the historical period and on the selected scenario for the 21st century period, as is done in the driving GCMs.

Of the nine CORDEX-CORE domains, here we focus on five areas of TC formation each covered by a different domain (Figure 2). We examine data for three 20-year periods, i.e. a reference historical period (1995–2014) and two future periods (2041–2060 and 2080–2099) for each scenario. Also, we compare the RegCM4 results with results from the driving GCMs, although due to the lack of some data for the RCP2.6 scenario, the GCM future runs are analyzed only for the RCP8.5. The TC characteristics analyzed, such as frequency, track density, intensity, lifetime and TC rainfall, are calculated for each simulation and each period separately. Then, ensemble averaged results are calculated by averaging of the individual simulations for each basin and period.

b. Data

To evaluate the simulated TCs, we use observed data from the International Best Track Archive for Climate Stewardship (IBTrACS, version v04; Knapp et al. 2010, 2018), which provides 6-hr data of TC locations, surface wind speed and central pressure from different basins. IBTrACS collects observed TC data from 11 agencies around the world covering all

major ocean basins where TCs occur: the North Atlantic (NA), Eastern Pacific (EP), western North Pacific (WP), North Indian Ocean (NI), South Indian Ocean (SI), and South Pacific (SP; Kruk et al. 2010). The minimum intensity reported by IBTrACS in each region varies from 25 kt (WP) to 30 kt (NA, EP) and 35 kt (NI, SI, SP), and here in order to facilitate a cross basin comparison we selected a common threshold of 17.5 m/s (~ 35 kt), which is used in the majority of the IBTrACS domains. Note that IBTrACS presents a homogeneous track dataset, with all non-10-min winds normalized to a 10-min average (Kruk et al. 2010).

For precipitation validation, we use the multi-source weighted-ensemble precipitation, version 2, (MSWEP – V2), a dataset based on a combination of rain-gauge measurements, satellite products and reanalysis data (Beck et al. 2017a, b). This dataset has shown good performance in describing precipitation over different regions around the world (Beck et al. 2017, 2019; Liu et al. 2019; Satgé et al. 2020) and has been used in global TC precipitation studies (Zhang et al. 2019).

c. Cyclone tracking

Tropical cyclone tracking is based on the objective feature-tracking algorithm TRACK (Hodges 1994; Hodges et al. 1995; Hodges 1999). This method has been widely used in previous studies for analyzing both tropical and extratropical cyclone tracks (Bengtsson et al. 2007, 2009; Manganello et al. 2012, 2014; Rastogi et al. 2018; Seiler et al. 2018). The algorithm initially identifies where grid point values of 6 hourly vertically averaged relative vorticity between 850 and 600 hPa are greater than 5×10^{-6} s^{-1} for the Northern Hemisphere (NH) and less than -5×10^{-6} s^{-1} for the Southern Hemisphere (SH) – at a spectral resolution of T63. These locations are refined using B-spline interpolation and greatest ascent maximization to find the off-grid

maxima/minima. Initially, all systems are tracked by first initializing a set of tracks using a nearest neighbor method and then refining the tracks by minimizing a cost function for track smoothness. Following tracking the T63 vorticity maxima/minima at all levels between 850 and 200hPa (850, 700, 600,500, 400, 300, 200hPa) are iteratively added to the tracks by searching for the extrema within a 5^0 radius (geodesic) of the cyclone centers. Additionally, the maximum 10-m wind within a 6^0 radius of the cyclone centers are added to the tracks. The TCs are initially identified from amongst all tracked features by applying criteria to detect a TC warm core, as a difference in the T63 vorticity field between 850 and 200 hPa greater than 6×10^{-5} s^{-1} and a vorticity maximum/minimum for all levels between 850 and 200 hPa for a coherent vertical structure and a maximum 10-m wind speed greater than 17.5 ms^{-1}. These criteria must be satisfied for at least one day over the oceans and the tracks must have lifetimes greater than 2 days. Furthermore, the maximum 10-m wind speed near the center of a cyclone must be greater than 17.5 ms^{-1} during the whole life cycle of the tropical cyclone. For the GCMs, instead of using 10-m wind data, which are not available, following Franklin et al (2003) and Walsh et al (2007) we use the maximum 850hPa wind speed near the center of the TC, with a threshold of 22 ms^{-1}.

d. Track density

The TC track density is defined for each 25 km grid point as the total number of days in a calendar year in which a storm center passes within a 500-km great circle distance of the grid point (Vecchi et al. 2014; Liu et al. 2018). The criteria for a 500-km storm size is used in observations and simulations and is consistent with previous TC studies (Chavas and Emanuel 2010; Barlow 2011; Prat and Nelson 2013; Khouakhi et al. 2017; and Liu et al. 2018).

e. TC intensity

At the present models' horizontal grid spacings (25 km for the RegCM4 and greater for the GCMs) it is impossible to reproduce observed cyclone wind intensities, which requires resolutions as fine as a few km (e.g. Gentry and Lackmann 2010). To overcome this systematic bias and adequately assess statistics of very intense tropical cyclones, the bias correction method used by Zhao and Held (2010) is applied to the simulated lifetime maximum 10 m wind speed (or 850hPa wind for the GCMs). This method adjusts the wind speed of a simulated TC to the wind speed of the observed TC with the same probability in the cumulative distribution function of maximum wind speed. For each basin, the adjustment is calculated using observations from the IBTrACS dataset. A comparison of observed TC intensities and RegCM4 results before the bias correction (Figure S1) showed that the simulations reproduce, and in fact in some basins overestimate, TCs of intensity less than 50 ms^{-1} but underestimate the occurrence of the most intense TCs.

f. TC rainfall

Here the TC rainfall is defined as the rainfall within a 500-km radius of each TC center. Similar to Zappa et al. (2015) and Liu et al. (2018), the total annual accumulated TC precipitation at a grid point can be expressed as $P = R \times F$, where P is the total storm rainfall, R is the average annual accumulated rainfall per storm, and F is the annual storm frequency expressed in days. Then, the change in rainfall related to TCs under GHG-induced warming can be directly attributed to the changes in the storm rainfall, or to the changes in storm frequency using $P' = R'F + RF' + R'F'$, where P' is the change of total storm rainfall, R' is the change in storm rainfall rate, and F' is the change in storm frequency. Therefore, the first and

second terms are contributions from storm rainfall rate and frequency, respectively, while the third term is the covariance effect, generally much smaller than the other terms (Liu et al. 2018).

Additionally, similar to Khouakhi et al. (2017), we assess the changes in the contribution of TCs to extreme rainfall using the peak-over-threshold (POT) method. For the POT calculation, at each grid point we compute the number of days exceeding the 95th percentile for rainy days (i.e. days with precipitation > 1mm), considering daily rainfall to be TC-induced only if the center of the storm is located within a 500-km radius of the grid point during a window of ±1 day.

3. Assessment of model simulated TCs

Figure 1 shows the mean annual cycle of TC frequency for the IBTrACS observations, GCMs and GCM-driven RegCM4 simulations during the reference period for the five basins highlighted by the boxes in Figure 2a. To determine the number of TCs in a particular month, we selected the time of maximum intensity in the simulations and IBTrACS. The observations show a peak of the TC season in August - September for the basins of the North and Eastern Pacific and North Atlantic Ocean, a double peak in the North Indian Ocean and a maximum in January through March over Australasia. The timing of seasonal peaks in TC activity are mostly reproduced by the RegCM4 simulations, although in some cases discrepancies of one month are found in the timing of the peak. Specifically, for the Northwest Pacific and North Atlantic basins the peak is shifted to September-October, while for the Eastern Pacific to July-August. These shifts mostly follow corresponding shifts in the driving GCMs, except over the Eastern Pacific. In addition, for the North Indian Ocean (Figure 1d), the RegCM4 simulations are not capable of producing the second maximum of TC activity, which is better captured by the MIROC5 GCM. In the other cases, the GCMs tend to severely underestimate the TC occurrence, except for the

261 MPI-ESM-MR and HadGEM2-ES models over Australasia. In the other basins, the RegCM4
262 simulations produce an annual TC frequency closer to the observed (IBTrACS) when compared
263 with the GCMs.

264 Considering the ensemble average, the RegCM4 simulations tend to overestimate the TC
265 frequency over the eastern North Pacific and Australasia, and to underestimate it over the
266 Northwest Pacific and North Indian Ocean. The model performance is poorest over the North
267 Indian Ocean (except for the MPI-driven runs), with the GCMs producing more TCs.
268 Importantly, in most cases the RegCM4 ensemble mean appear more consistent with IBTrACS
269 than the individual RegCM4 simulations, demonstrating the general usefulness of the ensemble
270 and its better reliability for this analysis.

271 For a quantitative assessment of the model in reproducing the TC frequency, Table 2
272 shows the correlation coefficients between the simulated (individual and ensemble GCMs and
273 RCMs) and observed (IBTrACS) annual cycle of TC frequency for each basin, along with the
274 mean annual absolute error (MAE) calcualted as the sum of the monthly MAE. For four of the
275 five basins in RegCM4, (except the North Indian Ocean) and three basins in the GCMs (except
276 the North Indian Ocean and the Northwestern Pacific), the correlations are quite high,
277 demonstrating a good performance by the individual simulations and the ensembles. The
278 ensembles mostly show intermediate MAE in comparison with the individual simulations, and in
279 comparison with the GCMs, the RegCM4 simulations show a better MAE over the North
280 Atlantic and Northwestern Pacific oceans. For the other basins the differences in correlation and
281 MAE across the two sets of models are small.

282 The geographic distribution of the TC track density for IBTrACS, GCM and RegCM4
283 simulations are shown in Figure 2a, 2b, and 2c, respectively. The observed track density shows

maxima in TC activity over the Northwest Pacific, tropical eastern Pacific, the ocean areas off the eastern coast of the United States, the Gulf of Mexico, the Bay of Bengal, and the tropical regions of Australia and adjacent oceans. The ensemble of GCMs is not able to reproduce the regions of maximum TC activity over the Northwest Pacific, tropical eastern Pacific and North Atlantic and overestimates the TC density over the Bay of Bengal and northwestern Australia.

The RegCM4 captures the spatial patterns of the TC climatology such as the maximum concentration over the tropical Eastern and Western Pacific, the western Atlantic, and northern Australia. The main model deficiency is the underestimation of TCs over the two cyclogenetic areas of the Indian Ocean, the Bay of Bengal and the Arabian Sea, areas where problems have been encountered also in previous studies (Manganello et al. 2012; Knutson et al. 2015; Bacmeister et al. 2018; Vishnu et al. 2019). The poor results in simulating TCs over the North Indian Ocean could be related to the difficulty in separating monsoon depressions from TCs in our tracking criteria and to a cold bias in sea surface temperature (SST) simulated over the North Indian Ocean in the GCMs (Supplementary Figure S2). Overall, Figure 2 shows that, compared to the GCMs, the RegCM4 simulates TC patterns which are closer to observations except for the two TC areas in the North Indian Ocean.

To investigate the physical processes underlying the TC frequency bias described in the GCMs above, we examine the bias (model minus ERA5 reanalysis) in SST, relative humidity at 700 hPa (RH700) and vertical wind shear (Vs) for the GCMs (Supplementary Figure S1). The underestimation in North Atlantic storms in the three GCMs can be potentially explained by the cold SST and dry RH700 biases in two of the models. Furthermore, the North Atlantic tropical cyclone genesis is strongly linked with tropical easterly waves, and these waves are not well represented in GCMs (Camargo et al, 2005). Similarly, the low production of TCs in the

307 NorESM1-M model over Australasia, Northwestern Pacific and North Indian Ocean can be
308 related to a cold SST bias there. The MPI-ESM-MR is the model with the smallest bias in SST
309 and RH700 and storm simulations closer to observations in all domains.

310 Figure 3 shows the mean annual TC frequency on the Saffir-Simpson hurricane wind
311 scale after the wind adjustment is carried out for both model ensembles. For the North Atlantic,
312 Northwest Pacific and Australasia (Figures 3a, e, b), the RegCM4 experiments in each category
313 are in line with the observations except for a systematic underestimation of tropical storms
314 (Category 0). For the Eastern Pacific, the RegCM4 ensemble mean overestimates TCs in all
315 categories, except Category 5, while over the North Indian Ocean (Figure 3d), as already
316 discussed, the RegCM4 ensemble simulations produce too few TCs. The GCM ensemble
317 severely underestimates TCs in all categories for the North Atlantic, Eastern Pacific and
318 Northwest Pacific basin, it overestimates TCs over the North Indian Ocean basin (except for
319 Category 0) and is comparable to observations over Australasia (again except for category 0).
320 Overall, the models tend to systematically underestimate category 0 events and to show more
321 mixed results for the other categories.

322 Figure 4 shows the storm duration in each basin. Overall, the RegCM4 experiments
323 simulate adequately the lifetime of the events and improve those generated by the GCMs over
324 Australasia, the Northwest Pacific and North Atlantic Ocean. Table 3 shows the correlation and
325 cumulated MAE between simulated (GCM and RCM ensembles) and observed (IBTrACS)
326 normalized frequencies in the life cycle of TCs over the regions identified in figure 2a. The
327 correlations for the RegCM4 ensemble are higher than the GCM ensembles in all basins,
328 indicating that the regional model reproduces better the observed life cycle distribution. For the
329 North Indian Ocean, the GCMs simulate better the long-lived events (Figure 4d) and also exhibit

330 a lower MAE than the RegCM4. In the Eastern Pacific (Figure 4c), neither the GCMs
331 (underestimate) nor the RegCM4 (overestimate) can reproduce adequately the duration of the
332 TCs, presenting relatively low correlations and high MAEs.

333 The average annual rainfall associated with TCs is displayed in Figure 5. The observed
334 climatology of TC rainfall (MSWEP) has the largest magnitude in the eastern United States,
335 southern Mexico, eastern China, Japan, northern Australia, eastern India and Bangladesh
336 (Figure 5a). This is supported by a higher TC density in these regions (Figure 2). The GCM
337 ensemble (Figure 5b) shows good agreement with observations at the coasts of the Bay of
338 Bengal and the South China Sea but a large underestimation of TC precipitation over the other
339 regions. The RegCM4 ensemble (Figure 5c) is generally closer to observations over the coastal
340 regions of central and south America, Australia a northeastern Asia, while it substantially
341 underestimates TC precipitation over the Bay of Bengal and Vietnam coasts.

342 Table 4 shows the correlation coefficients and spatial MAE between observed and
343 simulated TC precipitation. The correlations are generally high, in excess of 0.8, for both
344 ensembles, except for the RegCM4 over North India and the GCMs over the eastern Pacific. The
345 MAE values are lower for the RegCM4 than the GCMs over the North Atlantic and Australasia,
346 higher over the North Indian Ocean and comparable in the remaining two basins.

347 To quantify the relevance of cyclones for extreme precipitation events, we examined the
348 TC impact on extreme rainfall using the POT approach. Using the TC tracks from IBTrACS and
349 the MSWEP precipitation (Figure 6a), we find that Baja California and the Pacific Coast of
350 southwestern Mexico are the most affected by TC-induced heavy rainfall, where more than 45%
351 of the 95th percentile rainfall is TC-related. Other regions such as northwestern Australia,
352 eastern India, the southern part of the Arabian Peninsula, and Somalia (Figure 6a) show a large

353 contribution from TC-induced heavy rainfall, while in the southeastern United States and the
354 Caribbean region, values are in the range of 15% to more than 25% in the Yucatan Peninsula.

355 In general, the GCMs underestimate the contribution of TCs to extremes of precipitation
356 over northern Australia, North and Central America (Figures 6b, S3a) and overestimate it over
357 eastern Asia, but capture adequately the spatial pattern over Japan. Similar to the results for total
358 precipitation (Figure 5c), the RegCM4 simulations (Figures 6c, S3c) underestimate the TC
359 contribution to extreme rainfall over the North Indian Ocean and Australia. However, the
360 ensemble mean shows only a small underestimation along the southwestern Mexican coast and
361 the northern coasts of Australia, improving the GCMs results there. These results are consistent
362 with the correlations and bias shown in the Table 5. The general underestimation of TC-induced
363 precipitation can probably be attributed to the relatively low track density in the RegCM4
364 simulations compared with observations over coastal areas (Figure 2).

365 The spatial distribution of 95th-percentile precipitation (RR95p), as obtained from the
366 MSWEP observations and the GCM and RegCM4 ensembles, is presented in Fig. 7. In the
367 observed field (MSWEP, Fig. 7a), the highest values of 95th-percentile precipitation (RR95p)
368 appear over the Himalayan foothills, the western Indochina Peninsula, western India and
369 southern Japan. Both the GCMs and RegCM4 capture the main observed features of RR95p.
370 However, the GCMs (Figs. 7b, S3b) show a larger bias over eastern Asia, and an overestimation
371 over Australia and India, while the RegCM4 simulations (Figs. 7c, S3d) show an overestimation
372 in the Himalayas, Mexico and Central America and an underestimation over Australia and India.

373 In summary, the RegCM4 ensemble shows a relatively good performance in reproducing most of
374 the observed TC characteristics over the different basins analyzed, in several regions improving
375 the driving GCM results. The exception is the North Indian Ocean basin, where the regional

376 model underestimates TC occurrences and the GCM ensemble actually produces a better TC
377 climatology, especially in the second peak of the TC seasons.
378
379 **4. Future projections of TC characteristics**
380 In this section, we examine the changes in TC characteristics for the mid- (2041–2060)
381 and late (2080–2099) 21st century time slices relative to the baseline period (1995–2014) under
382 the RCP8.5 and RCP2.6 scenarios.
383 The projected changes in the TC seasonal cycle from the RegCM4 ensemble mean are
384 shown in Figure 8. For the North Atlantic (Figure 8a) and Australasia (Figure 8b), the
385 simulations project a prevailing decrease in TC occurrence, especially during the
386 climatologically active TC months (June to September in the Atlantic and February to April in
387 Australasia). For the RCP8.5 and the late future, the changes are statistically significant at the
388 95% confidence level, reaching a decrease in the North Atlantic of -2.3 and in Australasia of -4.6
389 TCs per year. For the Eastern Pacific (Figure 8c), North Indian Ocean (Figure 8d) and
390 northwestern Pacific (Figure 8e), the models show opposite trends, with a prevailing increase in
391 TC frequency, especially for the far future RCP8.5 (4.7, 0.85 and 4.3 TCs per year, respectively).
392 More specifically, we find a significant increase in TC activity in the Eastern Pacific during
393 August, November and December under the RCP8.5 scenario, while for the North Indian Ocean,
394 the largest and most significant changes occur in November and December, during the second
395 peak of TC activity. For the Northwest Pacific, the increase is shown during the peak of the
396 season (July-October). Hence, our results suggest an extension of the TC season in the Eastern
397 Pacific basin from April to December. Overall, our projected changes in the frequency of TCs
398 are qualitatively consistent with the changes found in the CMIP3 models (Knutson et al. 2010)

399 and with the CMIP5-RCP4.5 scenario (Knutson et al. 2015). Interestingly, the changes over the
400 North Indian Ocean and North Atlantic Ocean for the latter part of 21st century and the low-
401 emissions scenario are larger than those reported for the same period by Knutson et al. (2015).
402 The discrepancy among different results can be partly explained by differences in the design of
403 the experiments, tracking algorithms and subsets of CMIP5 models included in the studies.

404 The changes in the TC seasonal cycle from the GCMs (Figure 9) are generally similar to
405 those in the RegCM4 over the Eastern Pacific, North Atlantic and Australasia, but of smaller
406 magnitude. Conversely, for the North Indian and Northwest Pacific Ocean, the GCMs project a
407 decrease in the number of TCs during the peak season, opposite to those projected in the
408 RegCM4 simulations.

409 Figure 10 shows projected ensemble-mean changes in the spatial distributions of TC
410 occurrences as percentage change relative to the baseline period (1995-2014). Hatched areas
411 indicate where these changes are statistically significant at the 95% confidence level. For the
412 RCP8.5 scenario, the track densities in the RegCM4 experiments show consistent changes in the
413 two time slices, with greater magnitudes in the far future one: a strong and statistically
414 significant decrease over the Australasia region; a strong and statistically significant increase in
415 the northwestern Pacific; a decrease in the eastern Arabian Sea and, in the far future period, over
416 the Bay of Bengal; a prevailing decrease over the Gulf of Mexico, with an increase north of these
417 regions over the ocean areas off the coasts of the United States; a decrease over the eastern
418 Pacific coastal regions, with an increase further west over the ocean. These results are consistent
419 with those reported by Murakami et al. (2013, 2017) for the North Indian Ocean and Gleixner et
420 al. (2014) for Australasia. (about -20% and +40%, respectively).

Some of these patterns are similar in the RCP2.6, but with more mixed features. The results over the North Atlantic and Eastern Pacific mostly agree with previous simulations by Diro et al. (2014) and Knutson et al. (2015), with the exception of the northwestern part of the North Atlantic Ocean. Over this region, Knutson et al. (2015) found a decrease in TC frequency, in contrast to the increase shown in our results and in previous studies using a downscaling framework with CMIP3 (Emanuel 2008) and with CMIP5 data (Diro et al. 2014). Note that aside from the Australasia and Gulf of Mexico regions, the GCMs show patterns which are quite different from those of the RegCM4, often in fact of opposite sign, such as over the Bay of Bengal and the South China Sea.

Concerning landfalls, we find in the RegCM4, RCP8.5 scenario, significant and robust increases over the land surfaces bordering the South China Sea, such as Vietnam, southern China and for the far future over Philippines, where populations are already vulnerable to TC-induced flooding (Gupta 2010). In addition, in the late 21st century RCP8.5 there is a significant increase in TC density over the offshore areas northeast of the United States, indicating a greater potential for damage in this region, although a decrease is found over the Eastern U.S. in the mid-future slice.

Another important feature to consider is the impact of climate change on TC intensity. The changes in the ensemble mean annual TC frequency on the Saffir-Simpson Scale are shown in Figure 11. In general, the GCM and RegCM4 bias-adjusted model output shows either small or positive changes in the frequency of more intense (Categories 4 and 5) TCs in all basins, with prevailing positive changes in the RCP8.5 scenario, by 1.2, 3, 0.3 and 0.6 TCs/year over the North Atlantic, Eastern Pacific, North Indian Ocean and Northwest Pacific basins respectively. Over Australasia and the North Atlantic basin, the number of low-intensity TCs (Categories 0-2)

444 are significantly reduced in both ensembles in the RCP8.5, while for the Eastern Pacific an
445 increase in TCs is projected for all categories. Over the North Indian Ocean we find the largest
446 disagreement between RegCM4 and GCM projections, with opposite signs of changes between
447 the ensembles, while a generally mixed change response is finally seen in the Northwest Pacific.
448 In general, the results using winds without bias correction are in line with the bias corrected ones
449 (Supplementary Figure S4).

450 The increase in the occurrence of high-intensity TCs is consistent with Knutson et al.
451 (2015), who also project a large increase in TCs of categories 4-5 for the Eastern Pacific, North
452 Atlantic, Northwest Pacific and Arabian Sea. However, the RegCM4 results are opposite to those
453 of Knutson et al. (2015) over the northeastern Indian Ocean, where they report a decrease. These
454 differences could be related to different model resolutions and simulation design, although we
455 emphasize that the North Indian ocean is the region where the RegCM4 simulated TC statistics
456 show the lowest performance with respect to observations.

457 Figure 12 shows the RegCM4 ensemble-mean projected changes in TC duration, where
458 the values of TC duration are normalized with respect to the total number of TCs in each period.
459 Three of the five domains (North Atlantic, Australasia and Northwest Pacific) show a reduction
460 in the number of TCs with a long-life cycle, especially those lasting longer than seven days,
461 while the North Indian Ocean basin shows small changes and the Eastern Pacific an increase in
462 correspondence with a consistent reduction in the frequency of short-duration TCs. The results
463 for this latter basin are qualitatively in agreement with those of Emanuel et al. (2008). For the
464 other basins, the response of short-duration events shows mixed signals. The changes in TC
465 duration projected by the GCMs (Supplementary Figure S5) show more mixed results, but of

466 relevance is the fact that the GCM-produced responses are of opposite sign compared to the
467 RegCM4's over the Australasia and Eastern Pacific Basin.

468 Figure 13 shows the change of mean annual TC rainfall in the different periods and
469 scenarios for both the RegCM4 and GCM ensembles. In the RegCM4, under both scenarios, we
470 find a significant decrease over Australasia (hatched areas), by up to 60-90%, and over Mexico
471 and Central America by 20-40%, except for areas of northern Mexico. Over India, the Arabian
472 Peninsula, Myanmar, eastern China and Japan, the RCP8.5 RegCM4 projections show large
473 increases, significant in some regions, although this signal reverses sign in RCP2.6 in some areas
474 of southeastern China and northern Indochina Peninsula. The eastern coastal regions of the
475 United States show different changes depending on the forcing and period analyzed. Moving to
476 the GCM projections, in several cases changes are of opposite sign between the GCMs and
477 RegCM4, most noticeably over Australasia and southern Mexico.

478 Turning our attention to the changes in the TC contribution to extreme precipitation
479 (Figure 14), in the RegCM4, consistent with the differences in the rainfall rate, for all future
480 periods and scenarios, the percentage of extremes related to TCs primarily increases over the
481 North Indian Ocean, eastern China, Korea, and Japan by 20%. Over northern Australia, Mexico
482 and the eastern United States, our simulations indicate a prevailing, but not ubiquitous, decrease
483 in the percentage of high-precipitation events related to TCs, the change being larger for the
484 RCP8.5 and for the late future. Observational studies (Cavazos et al. 2008 and Pfahl and Wernli
485 2012) are consistent with these trends in the future projections. Again, the GCMs show some
486 instances of noticeably different responses, such as over Australasia and Mexico.
487

488 **5. Analysis of driving mechanisms**

The occurrence and development of TCs depends strongly on the SSTs and on characteristics of the large-scale environment such as vertical wind shear (Vs) and vertical thermodynamic profiles (Emanuel 1995). In general, the SST increases in the future, which should lead to increased TC occurrence and intensity. However, other atmospheric factors can drastically modulate this response and can help to explain the strongly basin-dependent responses found in the previous analysis.

Figure 15 presents the changes in large-scale environments over the different basins in the RegCM4 and GCM RCP8.5 simulations. The mean differences were calculated for the June-November season for the Atlantic, Western and Eastern Pacific basins, the November-March season for the Australasia domain and for the months of May, June, September-December for the North Indian Ocean. The first column shows the changes in vertical wind shear (Vs), defined as the vector difference of the wind at 850hPa and 200hPa. Excluding the influence of other environmental factors, high values in Vs are related to reduced TC activity and intensity (Frank and Ritchie 2001; Emanuel and Nolan 2004; Camargo et al. 2007).

Focusing on the RegCM4 runs first, there are prevailing decreases in Vs over the North Indian Ocean, the Gulf of Mexico, the eastern Pacific off the Mexican coast, the Florida/Caribbean region and the southeast Asia regions north of Australia i.e. favorable conditions for the increased TC activity. Over these regions, except north of Australia, the track densities indeed increase. Conversely, Vs increases across the Australia continent, over Central America and the south Gulf of Mexico and over the western Pacific off the coast of China, which is consistent with the reduced TC activity found over these regions (Figure 10d), with the exception of the eastern Pacific coastal areas. The projected changes in Vs, which appear to be an important factor driving the TC responses in the model, are broadly in line with those reported

512 by Vecchi and Soden (2007) and Murakami et al. (2012a), except over the northern part of the
513 Gulf of Mexico.

514 The second column shows changes in relative humidity at 700hPa (RH700), projecting a
515 consistent increase in mid-tropospheric RH over most regions except for the Northeastern Asia,
516 North of Australia and central America areas. In these latter two regions, this factor appears to be
517 dominant in inducing a decrease of TC activity (Figure 10d), a result in line also with Vecchi and
518 Soden (2007). Note that the changes over the Eastern Pacific are opposite to those documented
519 by Vecchi and Soden (2007) and Murakami et al. (2012a), but they are broadly consistent with
520 the changes in track density (Figure 10).

521 The third column shows the Maximum Potential Index (MPI; Emanuel 1995), i.e. the
522 maximum sustainable intensity of TCs based on the thermodynamics of the atmosphere and sea
523 surface. The RegCM4 simulations exhibit MPI increases over most TC regions (North Atlantic,
524 Eastern Pacific, North Indian and Northwest Pacific Ocean), possibly explaining the increase in
525 the frequency of the most intense TCs (Figure 11). However, for Australasia, the differences in
526 MPI between the future and historical periods are not homogenous throughout the basin. These
527 results are consistent with those obtained by Murakami et al. (2012a) and Camargo (2013) using
528 GCMs.

529 The change in the Genesis Potential Index (GPI; Emanuel and Nolan 2004) for
530 the ensemble mean is displayed in the last column. This is a metric that estimates the
531 potential for a TC to develop, combining the values of Vs, RH700, MPI, and large-scale
532 vorticity. Larger values of GPI are associated with enhanced tropical storm development. Model-
533 projected GPI increases modestly in the North Indian Ocean and Eastern Pacific but decreases in
534 the Caribbean and Australasia, consistent with the changes in the TC density (Figures 9 and 10).

However, over the central tropical Atlantic a statistically significant decrease in track density (Fig. 10d) is noted with negligible or increasing GPI (Fig. 15). Additionally, over the tropical Northwestern Pacific a strong increase in GPI occurs in the mid-future time period, but with slightly decreasing track density in the same region (Fig. 10a). In these regions it appears that large-scale forcings not captured by the GPI parameter are causing changes to the track density. For instance, over the central tropical Atlantic it is possible that a weakening of the west African monsoon may decrease the frequency of easterly waves which are the focus of tropical cyclone development over the central tropical Atlantic. Overall, the changes presented here for GPI are similar to the projections of Vecchi and Soden (2007) and Murakami et al. (2012a), with the exception of those for the Eastern Pacific. However, the RegCM4 projections for TC frequency over the Eastern Pacific agree with most recent studies using high-resolution models (Knutson et al. 2015; Bhatia et al. 2018).

A Similar analysis for the ensemble of the GCMs (bottom panels Figure 15), shows a prevailing, but not ubiquitous, consistency with the RegCM4 results. For both periods under the RCP8.5 scenario, there are increases in Vs and a reduction in the mid-troposphere RH over the North Atlantic Ocean, explaining the decrease in the tropical storm development in the GCMs (Figure 10f). Also, the MPI values show high values over the eastern Australian coast, consistent with the significant increase in the frequency of the most intense TC (Figure 11b), Finally, the inconsistencies in the changes in the TC activity between GCMs and RegCM4 found over the Bengal Bay and South China Sea can be explained by the projected changes in the RH700, for which the RegCM4 simulations produce a larger increase in the mid-troposphere, which then contributes to the simulated increase of TC activity.

The projected changes in seasonal mean SST and vertical wind shear from the five GCM analyzed are shown in Supplementary Figures S6 and S7, as they can help to explain the changes in the TC frequency. As expected, all the models show a global increase in SST in the range of 1-6 °C (Figure Supplementary S6), larger for the far future and for the RCP8.5 scenario. The largest warming is projected over the Northwestern Pacific and Northeastern basins, this latter showing also a significant increase in TC activity. Overall, the HadGEM2-ES produces the largest warming, particularly over the North Pacific Ocean.

Over the North Atlantic and Australasia, almost all the models, scenarios and periods exhibit an increase in vertical wind shear (Vs, Figure S7), while a decrease in Vs is found over the North Indian Ocean. All these changes are broadly consistent with the changes in TC frequency. For the Northwester Pacific, the changes in Vs are small in the south of the basin, while in the north they are not consistent across scenarios and periods. Similar results are found in the Northeastern Pacific Ocean.

6. Summary and Conclusions

The characteristics of TC activity over four CORDEX domains including 5 TC regions are examined for present and future climate conditions using the regional climate model RegCM4 driven by three GCMs. We analyze results from a series of simulations conducted as part of the CORDEX-CORE program at a horizontal grid spacing of 25 km for a historical period (1995–2014) and two future periods (2041–2060 and 2080–2099) under the RCP 2.6 and RCP 8.5 scenarios. Overall, the RegCM4 captures most of the features of the observed TC climatology, albeit with some systematic biases, such as an overestimate of TC density in the Eastern Pacific Ocean and an underestimate in the North Indian Ocean. In general, as expected

580 from its higher resolution, the RegCM4 generally shows an improved simulation of several TC
581 statistics compared to the driving GCMs in most basins, the main exception being the North
582 Indian Ocean, where the GCMs produce more TCs than RegCM4 especially in the second peak
583 season, more in line with observations.

584 Regarding the future scenarios, the changes in TC characteristics produced by RegCM4
585 indicate prevailing increases in TC frequency over the North Indian Ocean and the Eastern
586 Pacific, this latter region showing also a longer TC season in the future (from April to
587 December). These changes are consistent with the changes in GPI, particularly as related to an
588 increase in mid-tropospheric relative humidity. On the other hand, the North Atlantic and
589 Australasia basins show a decrease in TC frequency mostly associated with an increase in wind
590 shear over these basins. Over land, the changes in TC days show a prevailing increase in India
591 and decreases in Australia, Central America and Mexico. These results are qualitatively
592 consistent with a number of earlier studies (Emanuel et al. 2008; Lavender and Walsh 2011;
593 Murakami et al. 2013; Diro et al. 2014; Knutson et al. 2010, 2015; Bacmeister et al. 2018), but
594 they are opposite to those of Murakami et al. (2012b, 2014) over the northwest and northeast
595 Pacific. The main difference between the GCMs and RegCM4 TC responses occur over the
596 North Indian ocean basin, where the GCMs project a decrease in TC number.

597 The projections show a significant increase in the frequency of the strongest TCs over the
598 Eastern Pacific, the North Atlantic and the North Indian Ocean basins where the MPI has higher
599 values for all future scenarios (Murakami et al. 2012a). It is important to highlight that these
600 results are robust across the simulations using different driving GCMs for RCP8.5 scenario. Over
601 the northeast Pacific, Australasia and North Indian Ocean, the projected changes in the duration
602 of TCs in the RegCM4 are consistent with those documented by Webster et al. (2005) and

603 Emanuel et al. (2008) who showed a reduction in the number of long lasting TCs. However, the
604 GCM and RegCM4 ensembles show different responses over Australasia, where the GCMs
605 project a reduction in the frequency of short-duration TCs and an increase in those with a longer
606 lifetime.

607 The change in total annual TC rainfall exhibits a spatial pattern similar to that of the track
608 density, increasing significantly over the North India Ocean and decreasing in Australasia and
609 southern Mexico. We also find that future TCs will have a stronger effect on the upper part of
610 rainfall distribution over locations in the North Indian Ocean and northwestern Mexico,
611 consistent with trends observed by Cavazos et al. (2008) and Zhang and Zhou (2019). The
612 change in the TC rainfall rate exhibits an increase over Korea, Japan, India and the Arabian
613 Peninsula, and a mixed signal over the eastern coast of the United States and Central America. In
614 general, the GCM and RegCM4 ensembles show consistent signals in mean annual TC rainfall,
615 precipitation rate and contribution to extreme events, with the exception of Australia and
616 Mexico, where however, the GCMs have the largest bias in mean annual TC rainfall and TC
617 contribution to extreme precipitation during the historical period. A summary of the results for
618 the RegCM4 simulations is found in Table 6.

619 Our results clearly indicate that the issue of TC responses to increased GHG forcing is a
620 complex one, as it depends strongly on changes in the large-scale atmospheric environments
621 forcing TC formation, and thus it is highly basin-dependent. Future work should explore more in
622 detail the role of the vertical wind shear (Tran-Quang et al. 2020) and other environmental
623 factors (Emanuel et al. 2004) in future changes in TC intensity. Also, while we focused on cross
624 basin intercomparison of responses, more detailed analysis of individual basins might yield a

more in depth understanding of local driving mechanisms of changes in TC activity. Some robust and statistically significant responses were found in our study, often but not always in line with previous studies, and not always consistent between the RegCM4 and driving GCMs. This implies that a robust assessment of TC changes requires analyses of large ensembles of simulations with high resolution models driven by different GCMs capable of representing the response of different TC characteristics to critical atmospheric factors. Multi-model intercomparison projects such as CORDEX, HighResMIP and CMIP6 will thus provide increasingly valuable platforms to address this critical issue for society.

Acknowledgements

The RegCM4 simulations for the ICTP institute have been completed, thanks to the support of the CINECA supercomputing center, Bologna, Italy, and ISCRA projects HP10BDU7TR and HP10BQCFJ2. The authors would like to thank Graziano Giuliani and Ivan Girotto for their constant support in the preparation of the simulations used in this paper.

The authors would also like to thank the CMIP5 and Kevin Hodges, as well as the ESGF for providing access to their database, where most of the data was available. The study was also supported by the Oak Ridge Leadership Computing Facility, the National Climate-Computing Research Center at the Oak Ridge National Laboratory and the Chinese Academy of Sciences, all of whom provided access to their simulation data.

The observed data were provided by NOAA (https://www.ncdc.noaa.gov/ibtracs/index.php?name=bib) and by Hylke Beck, the developer of the MSWEP data (http://www.gloh2o.org/).

M. Reale has been supported in this work by OGS and CINECA under HPC-TRES award number 2015-07 and by the project FAIRSEA (Fisheries in the Adriatic Region—a Shared Ecosystem. Approach) funded by the 2014–2020 Interreg V-A Italy—Croatia CBC Programme (Standard project ID 10046951).

References

Arriaga-Ramírez S, Cavazos MT (2010) Regional trends of daily precipitation indices in northwest Mexico and southwest United States. J Geophys Res 115:1–10

Bacmeister, JT, Reed KA, Hannay C, Lawrence P, Bates S, Truesdale JE, Rosenbloom N, Levy M (2018) Projected changes in tropical cyclone activity under future warming scenarios using a high-resolution climate model. Clim Change 146:547–560. https://doi.org/10.1007/s10584-016-1750-x

Barlow M (2011) Influence of hurricane-related activity on North American extreme precipitation. Geophys Res Lett 38:L04705. https://doi.org/10.1029/2010GL046258

Beck HE, van Dijk AIJM, Levizzani V, Schellekens J, Miralles DG, Martens B, de Roo A (2017a) MSWEP: 3-hourly 0.25° global gridded precipitation (1979–2015) by merging gauge, satellite, and reanalysis data. Hydrol Earth Syst Sci 21:589–615

Beck HE et al (2017b) Global-scale evaluation of 22 precipitation datasets using gauge observations and hydrological modeling. Hydrol Earth Syst Sci 21:6201–6217

Beck HE et al. (2019) Daily evaluation of 26 precipitation datasets using Stage-IV gauge-radar data for the CONUS. Hydrol Earth Syst Sc 23:207–224. https://doi.org/10.5194/hess-23-207-2019

Bengtsson, L, Hodges KI, Esch M, Keenlyside N, Kornblueh L, Luo J-J, Yamagata

676 T (2007) How may tropical cyclones change in a warmer climate? Tellus 59A:539–561
677
678 Bengtsson L, Hodges KI, Keenlyside N (2009) Will extratropical storms intensify in a warmer
679 climate? J Clim 22(9):2276–2301. doi: 10.1175/2008jcli2678.1
680
681 Bhatia K, Vecchi G, Murakami H, Underwood S, Kossin J (2018) Projected response of tropical
682 cyclone intensity and intensification in a global climate model. J Clim 31:8281-8303.
683 https://doi.org/10.1175/JCLI-D-17-0898.1
684
685 Bretherton CS, McCaa JR, Grenier H (2004) A new parameterization for shallow cumulus
686 convection and its application to marine subtropical cloud-topped boundary layers. I. Description
687 and 1D results. Mon Weather Rev 132:864–882
688
689 Camargo SJ, Emanuel KA, Sobel AH (2007) Use of a genesis potential index to diagnose ENSO
690 effects on tropical cyclone genesis. J Clim 20:4819–4834
691
692 Camargo SJ (2013) Global and regional aspects of tropical cyclone activity in the CMIP5
693 models. J Clim 26:9880–9902. doi: http://dx.doi.org/10.1175/JCLI-D-12-00549.1
694
695 Camargo SJ, Wing AA (2016) Tropical cyclones in climate models. WIREs Climate Change,
696 7:211-237. doi: 10.1002/wcc373
697
698 Cavazos T, Turrent C, Lettenmaier DP (2008) Extreme precipitation trends associated with
699 tropical cyclones in the core of the North American monsoon. Geophys Res Lett 35:L21703
700
701 Chavas DR, Emanuel KA (2010) A QuikSCAT climatology of tropical cyclone size. Geophys
702 Res Lett. 37:L18816. https://doi.org/10.1029/2010GL044558
703
704 Christensen JH, Krishna Kumar K, Aldrian E, An S-I, Cavalcanti IFA, de Castro M, Dong W,
705 Goswami P, Hall A, Kanyanga JK, Kitoh A, Kossin J, Lau N-C, Renwick J, Stephenson DB, Xie
706 S-P, Zhou T (2013) Climate Phenomena and their Relevance for Future Regional Climate

Change. In: Climate Change 2013: The Physical Science Basis. Contribution of Working Group I to the Fifth Assessment Report of the Intergovernmental Panel on Climate Change. [Stocker, T.F., D. Qin, G.-K. Plattner, M. Tignor, S. K. Allen, J. Boschung, A. Nauels, Y. Xia, V. Bex, P. M. Midgley.], Cambridge University Press, 1535 pp

Collins WJ, Bellouin N, Doutriaux-Boucher M, Gedney N, Halloran P, Hinton T, Hughes J, Jones CD, Joshi M, Liddicoat S, Martin G, O'Connor F, Rae J, Senior C, Sitch S, Totterdell I, Wiltshire A, Woodward S (2011) Development and evaluation of an Earth-System model-HadGEM2. GMD 4:1051–1075. doi:f10.5194/gmd-4-1051-2011g

Czajkowski J, Villarini G, Michel-Kerjan E, Smith JA (2013) Determining tropical cyclone inland flooding loss on a large scale through a new flood peak ratio-based methodology. Environ Res Lett 8:044056. doi:10.1088/1748-9326/8/4/044056

Diro, GT, Giorgi F, Fuentes-Franco R, Walsh KJE, Guliani G, Coppola E (2014) Tropical cyclones in a regional climate change projection with RegCM4 over the CORDEX Central America domain. Clim Change 125:79–94. doi:10.1007/s10584-014-1155-7

Dominguez C, Magaña V (2018) The role of tropical cyclones in precipitation over the tropical and subtropical North America. Front Earth Sci 6:19. https://doi.org/10.3389/feart.2018.00019

Dunne JP et al (2012) GFDL's ESM2 global coupled climate-carbon earth system models. Part I: physical formulation and baseline simulation characteristics. J Clim 25:6646–6665

Elguindi N, Giorgi F, Turuncoglu UU (2014) Assessment of CMIP5 global model simulations over the sub-set of CORDEX domains used in the Phase I CREMA Experiment. Climatic Change. doi: 10.1007/S10584-013-0935-9

Emanuel K (1991) A scheme for representing cumulus convection in large scale models. J Atmos Sci 48:2313–2335

738 Emanuel KA (1995) Sensitivity of tropical cyclones to surface exchange coefficients and a
739 revised steady-state model incorporating eye dynamics. J Atmos Sci 52:3969– 3976
740
741 Emanuel KA, Nolan D (2004) Tropical cyclone activity and the global climate system. Preprints,
742 26th Conf. on Hurricanes and Tropical Meteorology, Miami, FL, Amer Meteor Soc 10 A.2.
743 [Available online at https://ams.confex.com/ams/26HURR/techprogram/paper_75463.htm.]
744
745 Emanuel KA, DesAutels C, Holloway C, Korty R (2004) Environmental control of tropical
746 cyclone intensity. J Atmos Sci 61:843–858
747
748 Emanuel KA, Sundararajan R, Williams J (2008) Hurricanes and global warming: Results from
749 downscaling IPCC AR4 simulations. Bull Amer Meteor Soc 89:347–367
750
751 Frank WM, Ritchie EA (2001) Effects of vertical wind shear on the intensity and structure of
752 numerically simulated hurricanes. Mon Wea Rev 129:2249 -2269
753
754 Franklin JL, Black ML, Valde K (2003) GPS dropwindsonde wind profiles in hurricanes and
755 their operational implications. Weather Forecast 18:32–44
756
757 Fuentes-Franco R, Giorgi F, Coppola E, Zimmermann K (2017) Sensitivity of tropical cyclones
758 to resolution, convection scheme and ocean flux parameterization over Eastern Tropical Pacific
759 and Tropical North Atlantic Oceans in the RegCM4 model. Clim Dyn 49(1–2):547–561
760
761 Gentry MS, Lackmann GM (2010) Sensitivity of simulated tropical cyclone structure and
762 intensity to horizontal resolution. Mon Wea Res 138:688-704.
763
764 Giorgi F, Jones C, Asrar GR (2009) Addressing climate information needs at the regional level:
765 the CORDEX framework. WMO Bull 58(3):175–183
766
767 Giorgi F, Coppola E, Solmon F, Mariotti L and others (2012) RegCM4: Model description and
768 preliminary tests over multiple CORDEX domains. Clim Res 52:7–29

Giorgi F, Gutowski WJ (2015) Regional dynamical downscaling and the CORDEX initiative. Annu Rev Environ Resour 40:467–490

Giorgi F (2019) Thirty years of regional climate modeling: where are we and where are we going next? J Geophys Res Atmos 124:5696–5723

Gleixner S, Keenlyside N, Hodges KI et al (2014) An inter-hemispheric comparison of the tropical storm response to global warming. Clim Dyn 42:2147–2157. https://doi.org/10.1007/s00382-013-1914-6

Grell GA, Dudhia J, Stauffer D (1994) A description of the fifth-generation Penn State/NCAR mesoscale model (MM5). Technical report NCAR/TN-398 + STR, National Center for Atmospheric Research

Gutowski WJ Jr, Giorgi F, Timbal B, Frigon A, Jacob D, Kang HS, Raghavan K, Lee B, Lennard C, Nikulin G, O'Rourke E, Rixen M, Solman S, Stephenson T, Tangang F (2016) WCRP coordinated regional downscaling experiment (CORDEX): a diagnostic MIP for CMIP6. Geosci Model Dev 9:4087–4095. https://doi.org/10.5194/gmd-9-4087-2016

Hodges KI (1994) A general method for tracking analysis and its application to meteorological data. Mon Weather Rev 122:2573– 2586

Hodges KI (1995) Feature tracking on the unit sphere. Mon Weather Rev 123:3458– 3465

Hodges KI (1999) Adaptive constraints for feature tracking. Mon Weather Rev 127:1362– 1373

Holtslag A, de Bruijn E, Pan H-L (1990) A high resolution air mass transformation model for short range weather forecasting. Mon Weather Rev 118:1561–1575

Hsu, WC, Patricola CM, Chang P (2019) The impact of climate model sea surface temperature

biases on tropical cyclone simulations. Clim Dyn 53: 173. https://doi.org/10.1007/s00382-018-4577-5

Jin C-S, Cha D-H, Lee D-K, Suh M-S, Hong S-Y, Kang H-S, Ho C-H (2016) Evaluation of climatological tropical cyclone activity over the western North Pacific in the CORDEX-East Asia multi-RCM simulations. Clim Dyn 47:765– 778. https://doi.org/10.1007/s00382-015-2869-6

Kain J-S (2004) The Kain–Fritsch convective parameterization: an update. J Appl Meteorol 43(1):170–181

Kain J-S, Fritsch J-M (1990) A one-dimensional entraining/detraining plume model and its application in convective parameterization. J Atmos Sci 47(23):2784–2802

Khouakhi A, Villarini G, Vecchi GA (2017) Contribution of Tropical Cyclones to Rainfall at the Global Scale. J Climate 30:359–372. https://doi.org/10.1175/JCLI-D-16-0298.1

Knapp KR, Kruk MC, Levinson DH, Diamond HJ, Neumann CJ (2010)
The International Best Track Archive for Climate Stewardship (IBTrACS): Unifying tropical cyclone best track data. Bull Amer Meteor Soc 91:363-376. doi:10.1175/2009BAMS2755.1

Knapp KR, Diamond HJ, Kossin JP, Kruk MC, Schreck CJ (2018) International Best Track Archive for Climate Stewardship (IBTrACS) Project, Version 4. NOAA National Centers for Environmental Information. https://doi.org/10.25921/82ty-9e16 [accessed 10/09/2019]

Knutson TR, McBride JL, Chan JCL, Emanuel KA, Holland GJ, Landsea C, Held IM, Kossin JP, Srivastava AK, Sugi M (2010) Tropical cyclones and climate change. Nat Geosci 3(3):157–163. https://doi.org/10.1038/ngeo779

Knutson TR, Sirutis JJ, Vecchi GA, Garner S, Zhao M, Kim H-S, Bender M, Tuleya RE, Held IM, Villarini G (2013) Dynamical downscaling projections of late 21st century Atlantic

831 hurricane activity: CMIP3 and CMIP5 model-based scenarios. J Clim 26:6591-6617. DOI:
832 10.1175/JCLI-D-12-00539.1
833
834 Knutson TR et al (2015) Global Projections of Intense Tropical Cyclone Activity for the Late
835 Twenty-First Century from Dynamical Downscaling of CMIP5/RCP4.5 Scenarios. J Clim
836 28(18). doi: 10.1175/JCLI-D-15-0129.1
837
838 Knutson T, Camargo SJ, Chan JC, Emanuel K, Ho C, Kossin J, Mohapatra M, Satoh M, Sugi M,
839 Walsh K, Wu L (2019) Tropical Cyclones and Climate Change Assessment: Part I: Detection
840 and Attribution. Bull Amer Meteor Soc 100:1987-2007. https://doi.org/10.1175/BAMS-D-18-
841 0189.1
842
843 Knutson T, Camargo SJ, Chan JC, Emanuel K, Ho C, Kossin J, Mohapatra M, Satoh M, Sugi M,
844 Walsh K, Wu L (2020) Tropical cyclones and climate change assessment: Part II. projected
845 response to anthropogenic warming. Bull Amer Meteor Soc. https://doi.org/10.1175/BAMS-D-
846 18-0194.1
847
848 Kruk MC, Knapp KR, Levinson DH (2010) A Technique for Combining Global Tropical
849 Cyclone Best Track Data. J Atmos Oceanic Technol 27:680–
850 692. https://doi.org/10.1175/2009JTECHA1267.1
851
852 Lavender SL, Walsh KJE (2011) Dynamically downscaled simulations of Australian region
853 tropical cyclones in current and future climates. Geophys Res Lett 38.
854 doi:10.1029/2011GL047499
855
856 Li T, Kwon M, Zhao M, Kug J-S, Luo J-J, Yu W (2010) Global warming shifts Pacific tropical
857 cyclone location. Geophys Res Lett 37:L21804
858
859 Liu J, Shangguan D, Liu S, Ding Y, Wang S, Wang X (2019) Evaluation and comparison of
860 CHIRPS and MSWEP daily-precipitation products in the Qinghai-Tibet Plateau during the

861 period of 1981–2015. Atmos Res 230 104634.
862
863 Liu M, Vecchi GA, Smith JA, Murakami H (2018) Projection of Landfalling–Tropical Cyclone
864 Rainfall in the Eastern United States under Anthropogenic Warming. J Clim 31:7269–
865 7286. https://doi.org/10.1175/JCLI-D-17-0747.1
866
867 Manganello JV, Hodges KI, Kinter JL, Cash BA, Marx L, Jung T, Achuthavarier D, Adams
868 JM, Altshuler EL, Huang B, Jin EK, Stan C, Towers P, Wedi N (2012) Tropical cyclone
869 climatology in a 10 km global atmospheric GCM: Toward weather-resolving climate modeling. J
870 Clim 25:3867– 3893
871
872 Manganello JV, Hodges KI, Dirmeyer B, Kinter JL, Cash BA, Marx L, Jung T, Achuthavarier
873 D, Adams JM, Altshuler EL, Huang B, Jin EK, Towers P, Wedi N (2014) Future changes in the
874 western North Pacific tropical cyclone activity projected by a multidecadal simulation with a 16-
875 km global atmospheric GCM. J Clim 27:7622– 7646. https://doi.org/10.1175/JCLI-D-13-
876 00678.1
877
878 Martínez-Sanchez JN, Cavazos T (2014) Eastern Tropical Pacific hurricane variability and
879 landfalls on Mexican coasts. Clim Res 58, 221-234
880
881 Moss R et al (2008) Towards new scenarios for analysis of emissions, climate change, impacts,
882 and response strategies. Intergovernmental Panel on Climate Change, Geneva, 132 pp
883
884 Murakami H, Wang Y, Yoshimura H, Mizuta R, Sugi M, Shindo E, Adachi Y, Yukimoto S,
885 Hosaka M, Kusunoki S, Ose T, Kitoh A (2012a) Future changes in tropical cyclone activity
886 projected by the new high-resolution MRI-AGCM. J Clim 25:3237-3260
887
888 Murakami H, Mizuta R, Shindo E (2012b) Future changes in tropical cyclone activity projected
889 by multi-physics and multi-SST ensemble experiments using the 60-km-mesh MRI AGCM.
890 Clim Dyn 39(9-10):2569-2584
891

892 Murakami H, Sugi M, Kitoh A (2013) Future changes in tropical cyclone activity in the North
893 Indian Ocean projected by high-resolution MRI-AGCMs. Clim Dyn 40:1949–1968.
894 doi:10.1007/s00382-012-1407-z
895
896 Murakami H, Hsu P-C, Arakawa O, Li T (2014) Influence of model biases on projected future
897 changes in tropical cyclone frequency of occurrence. J Clim 27:2159–2181
898
899 Murakami HG, Vecchi A, Underwood S (2017) Increasing frequency of extremely severe
900 cyclonic storms over the Arabian Sea. Nat Clim Change 7:885–889
901
902 Pal J-S, Small E-E, Eltahir E-A-B (2000) Simulation of regional scale water and energy budgets:
903 representation of subgrid cloud and precipitation processes within RegCM. J Geophys Res
904 105(D24):29579–29594
905
906 Papalexiou, SM, Montanari A (2019) Global and regional increase of precipitation extremes
907 under global warming. Water Resour Res 55:4901– 4914
908
909 Pfahl, S, Wernli H (2012) Quantifying the relevance of cyclones for precipitation extremes. J
910 Clim 25:6770–6780
911
912 Prat OP, Nelson BR (2013) Mapping the world's tropical cyclone rainfall contribution over land
913 using the TRMM Multi-satellite Precipitation Analysis. 49:7236-7254.
914 https://doi.org/10.1002/wrcr.20527
915
916 Rappaport EN (2000) Loss of life in the United States associated with recent Atlantic tropical
917 cyclones. Bull Amer Meteor Soc 81:2065–2073, doi:10.1175/1520-0477(2000)0812.3.CO;2
918
919 Rastogi D, Ashfaq M, Leung R, Ghosh S, Saha A, Hodges K, Evans K (2018), Characteristics of
920 Bay of Bengal, Monsoon Depressions in the 21st Century. Geophys Res Lett.
921 https://doi.org/10.1029/2018GL078756.
922

923 Reed KA, Bacmeister JT, Rosenbloom NA et al (2015) Impact of the dynamical core on the
924 direct simulation of tropical cyclones in a high-resolution global model. Geophys Res Lett
925 42:3603–3608. https://doi.org/10.1002/2015GL063974
926
927 Satgé F, Defrance D, Sultan B, Bonnet, MP, Seyler F, Rouché N, Pierron F, Paturel JE (2020)
928 Evaluation of 23 gridded precipitation datasets across West Africa. J Hydrol 581 124412
929
930 Seiler C, Zwiers F, Hodges KI, Scinocca J (2018) How does dynamical downscaling affect
931 model biases and future projections of explosive extratropical cyclones along North America's
932 Atlantic coast? Clim Dyn 50:677–692. https://doi.org/10.1007/s00382-017-3634-9
933
934 Sugi M, Murakami H, Yoshida K (2017) Projection of future changes in the frequency of intense
935 cyclones. Clim Dyn 49:619–632. https://doi.org/10.1007/s00382-016-3361-7
936
937 Taylor KE, Stouffer RJ, Meehl GA (2012) An overview of CMIP5 and the experiment design.
938 Bull Am Meteorol Soc 78:485–498
939
940 Tiedtke M (1996) An extension of cloud-radiation parameterization in the ECMWF model: the
941 representation of subgrid-scale variations of optical depth. Mon. Weather Rev. 124:745–
942 750. https://doi.org/10.1175/1520-0493(1996)124%3C0745:AEOCRP%3E2.0.CO;2
943
944 Tran-Quang D, Pham-Thanh H, Vu T, Kieu C, Phan-Van T (2020) Climatic Shift of the Tropical
945 Cyclone Activity Affecting Vietnam's Coastal Region. J Appl Meteor Climatol 59:1755–
946 1768. https://doi.org/10.1175/JAMC-D-20-0021.1.
947
948 Vecchi GA, Soden BJ (2007) Increased tropical Atlantic wind shear in model projections of
949 global warming. Geophys Res Lett 34:L08702
950
951 Vecchi GA, Delworth T, Gudgel R, Kapnick S, Rosati A, Wittenberg AT, Zeng F, Anderson W,
952 Balaji V, Dixon K, Jia L, Kim H, Krishnamurthy L, Msadek R, Stern WF, Underwood SD,
953 Villarini G, Yang X, Zhang S (2014) On the Seasonal Forecasting of Regional Tropical Cyclone

954 Activity. J Clim 27:7994–8016. https://doi.org/10.1175/JCLI-D-14-00158.1
955
956 Vishnu S, Sanjay J, Krishnan R (2019) Assessment of climatological tropical cyclone activity
957 over the north Indian Ocean in the CORDEX-South Asia regional climate models. Clim Dyn 53:
958 5101. https://doi.org/10.1007/s00382-019-04852-8
959
960 Walsh KJE, Fiorino M, Landsea CW, McInnes KL (2007) Objectively determined resolution-
961 dependent threshold criteria for the detection of tropical cyclones in climate model and
962 reanalyses. J Clim 20:2307–2314
963
964 Walsh K, Lavender S, Murakami H, Scoccimarro E, Caron L-P, Ghantous M (2010) The tropical
965 intercomparison project. In: Elsner JB, Hodges RE, Malmstadt JC, Scheitlin KN (eds)
966 Hurricanes and climate change. Springer, Berlin, pp 1–24
967
968 Walsh, K. J. E., J. L. McBride, P. J. Klotzbach, S. Balachandran, S. J. Camargo, G. Holland, T.
969 R. Knutson, J. P. Kossin, T-C Lee, A. Sobel and M. Sugi, (2016) Tropical cyclones and climate
970 change. Wiley Interdisciplinary Reviews: Climate Change 7(1). DOI:10.1002/wcc.371
971
972 Wang C, Liang J, Hodges KI. (2017) Projections of tropical cyclones affecting Vietnam under
973 climate change: Downscaled HadGEM2-ES using PRECIS 2.1. Q J R Meteorol
974 Soc. https://doi.org/10.1002/qj.3046
975
976 Watanabe M et al (2010) Improved climate simulation by MIROC5: Mean states, variability, and
977 climate sensitivity. J Clim 23:6312–6335
978
979 Webster PJ, Holland GJ, Curry JA, Chang HR (2005) Changes in tropical cyclone number,
980 duration, and intensity in a warming environment. Science 309(5742):1844–1846.
981 doi:10.1126/science.1116448
982
983 Wehner MF, Reed KA, Loring B, Stone D, Krishnan H (2018) Changes in tropical cyclones
984 under stabilized 1.5 °C and 2.0 °C global warming scenarios as simulated by the Community

Atmospheric Model under the HAPPI protocols. Earth Syst Dyn 9:187–195

Zanchettin D, Rubino A, Matei D, Jungclaus JH (2013) Multidecadal-to-centennial SST variability in the MPI-ESM simulation ensemble for the last millennium. Clim Dyn 40(5):1301–1318. doi:10.1007/s00382-012-1361-9

Zappa G, Hawcroft MK, Shaffrey L, Black E, Brayshaw DJ (2015) Extratropical cyclones and the projected decline of winter Mediterranean precipitation in the CMIP5 models. Clim Dyn 45:1727–1738

Zeng X, Zhao M, Dickinson R-E (1998) Intercomparison of bulk aerodynamic algorithms for the computation of sea surface fluxes using TOGA COARE and TAO data. J Clim 11(10):2628–2644

Zhang W, Villarini G, Vecchi GA, Murakami H (2019) Rainfall from tropical cyclones: high-resolution simulations and seasonal forecasts. Clim Dyn. https://doi.org/10.1007/s00382-018-4446-2

Zhang W, Zhou T (2019) Significant Increases in Extreme Precipitation and the Associations with Global Warming over the Global Land Monsoon Regions. J Clim 32:8465–8488. https://doi.org/10.1175/JCLI-D-18-0662.1

Zhang ZS et al (2012) Pre-industrial and mid-Pliocene simulations with NorESM-L. Geosci Model Dev 5:523–533. doi:10.5194/gmd-5-523-2012

Zhao M, Held IM (2010) An analysis of the effect of global warming on the intensity of Atlantic hurricanes using a GCM with statistical refinement. J Clim 23:6382– 6393

List of Figures

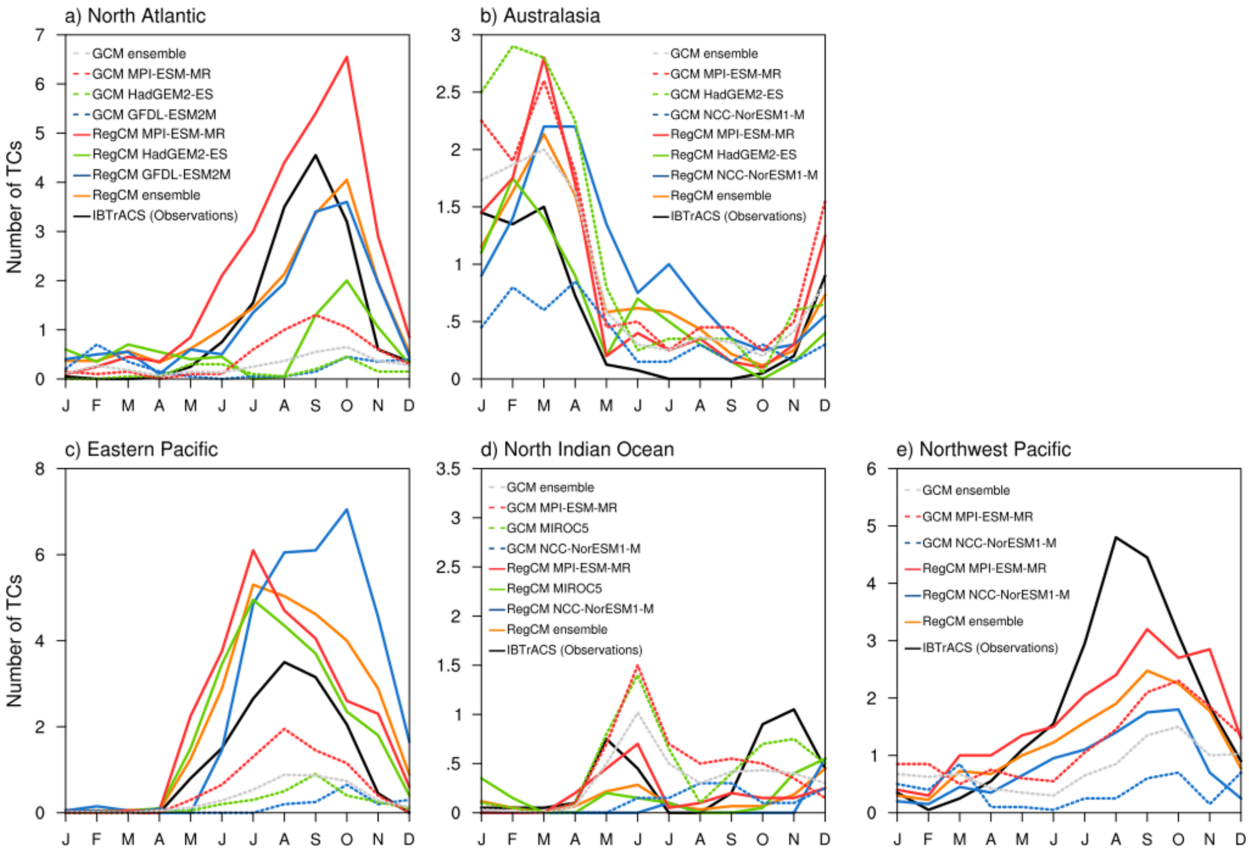

Figure 1. TC annual cycle over the a) North Atlantic, b) Australasia, c) the Eastern Pacific, d) the North Indian and e) Northwest Pacific Ocean during 1995-2014.

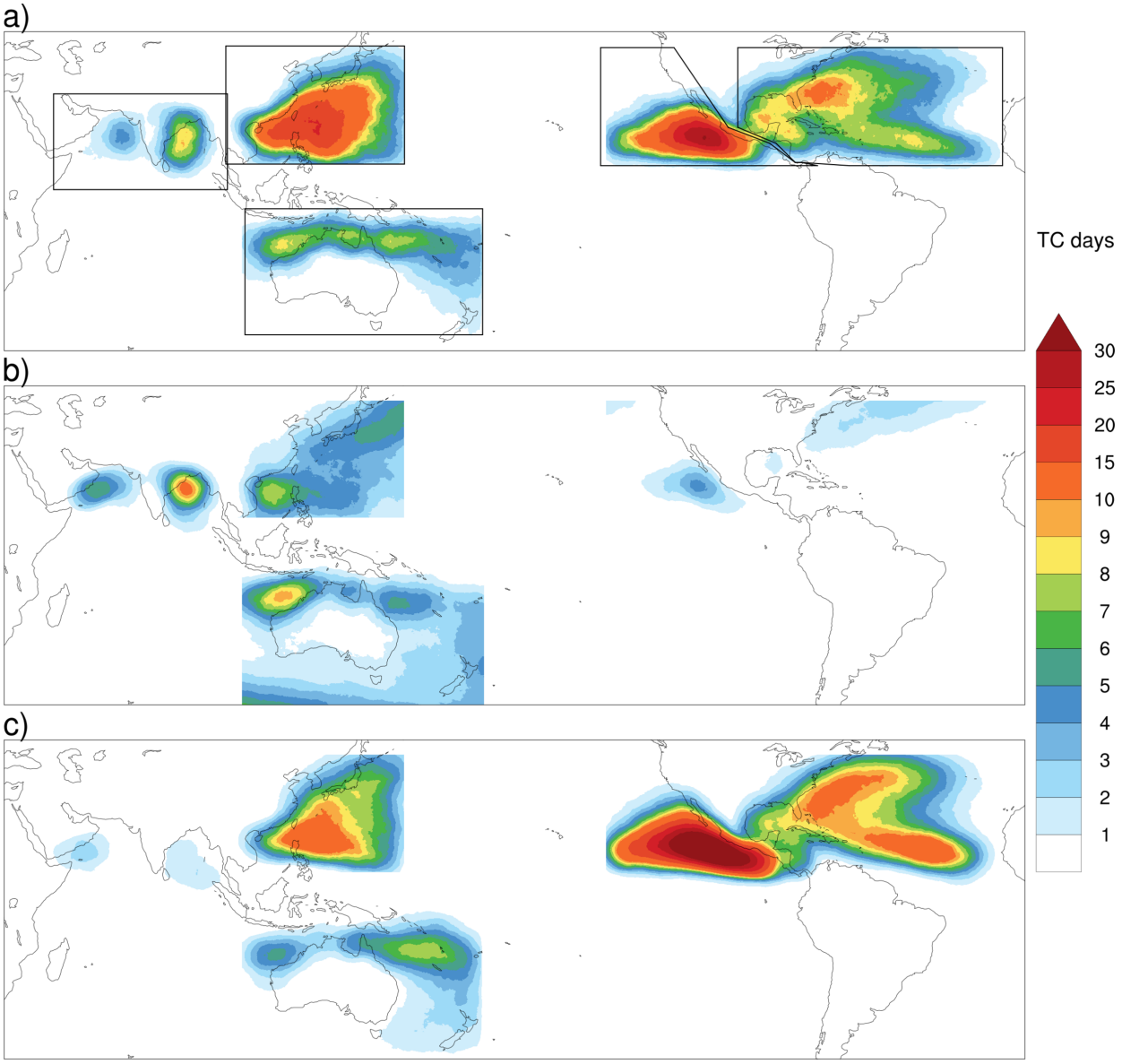

Figure 2. TC track density (TC days in a calendar year in which a storm center passes within a 500-km great circle distance of the grid point) from a) IBTrACS, b) GCM ensemble mean and c) RegCM ensemble mean.

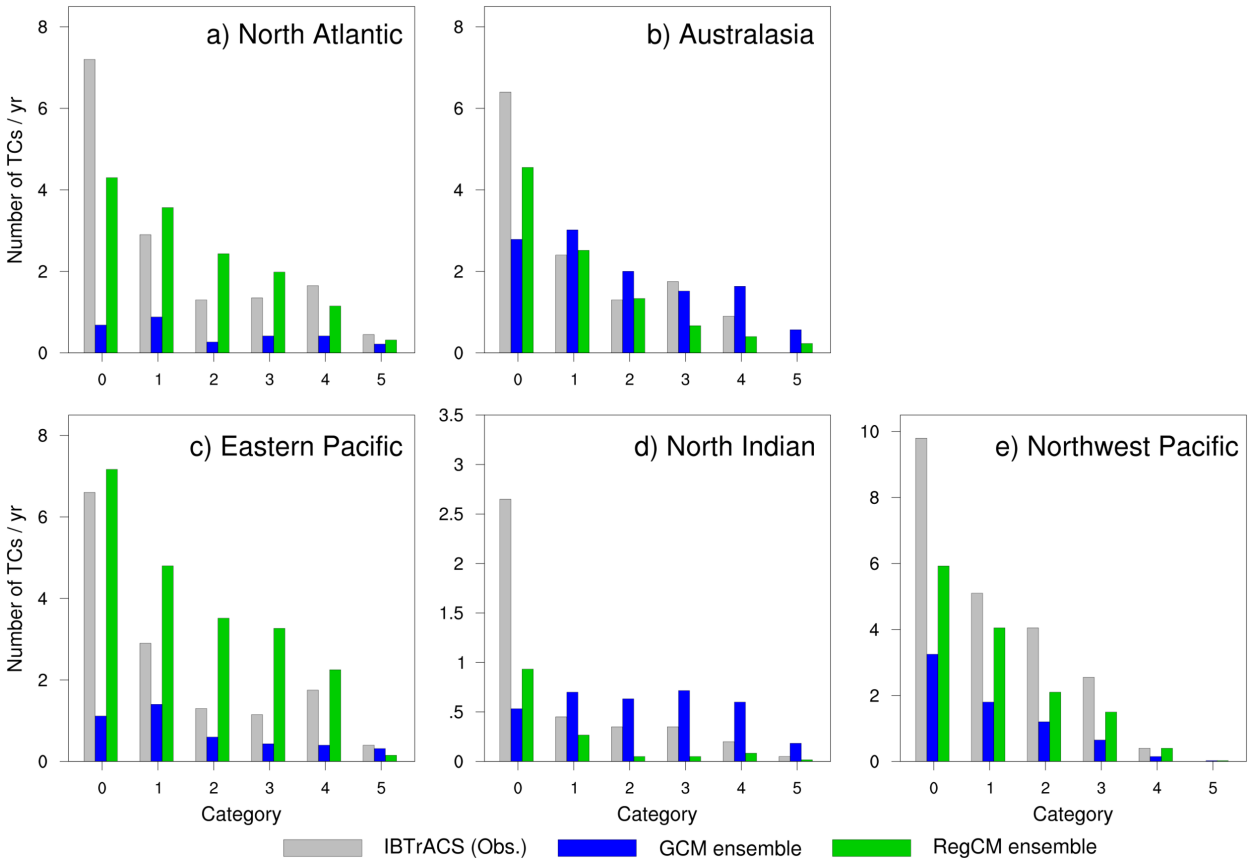

Figure 3. Annual number of TCs categorized by the Saffir-Simpson scale (before bias correction) for the a) North Atlantic, b) Australasia, c) the Eastern Pacific, d) the North Indian and e) Northwest Pacific Ocean for 1995-2014. Category 0 refers to storms of Tropical Storm intensity.

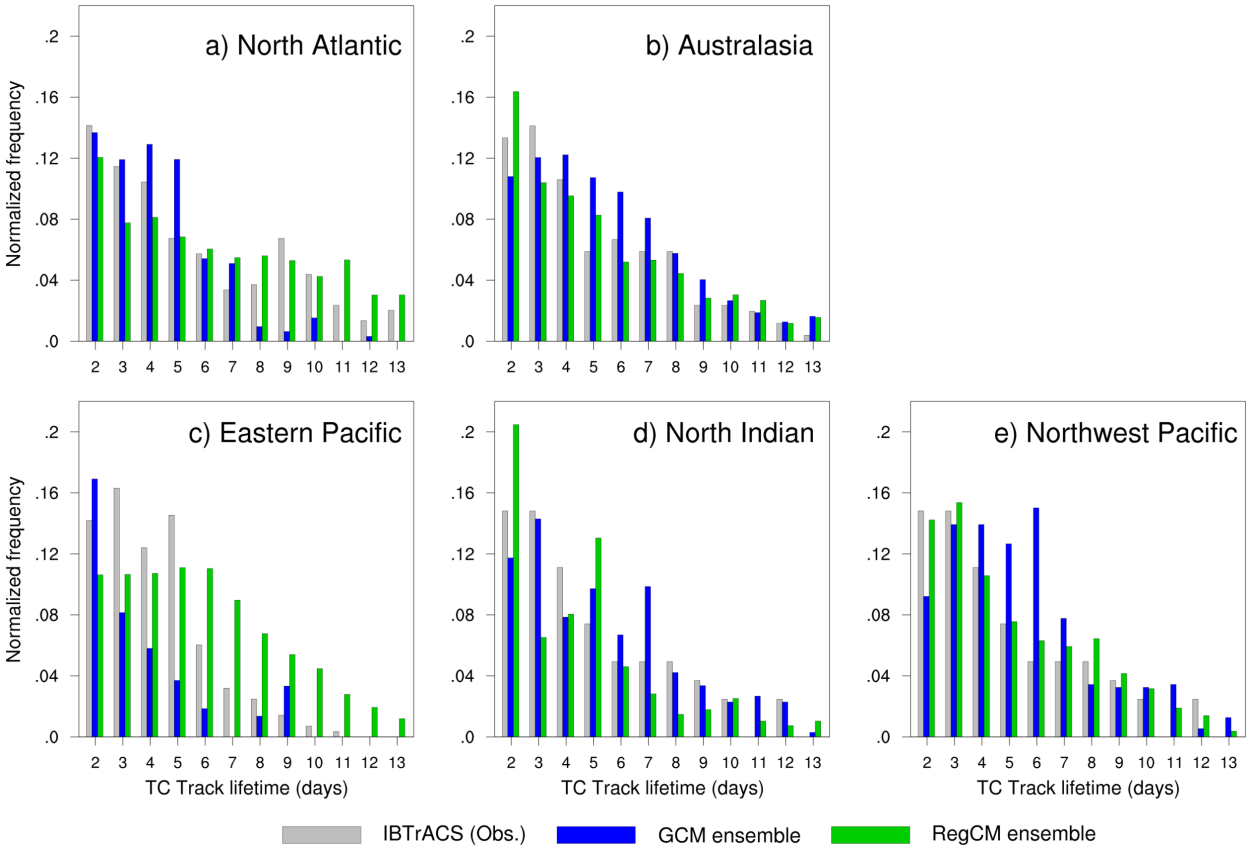

Figure 4. Normalized frequency in the life cycle of TCs for the a) North Atlantic, b) Australasia, c) the Eastern Pacific, d) the North Indian and e) Northwest Pacific Ocean.

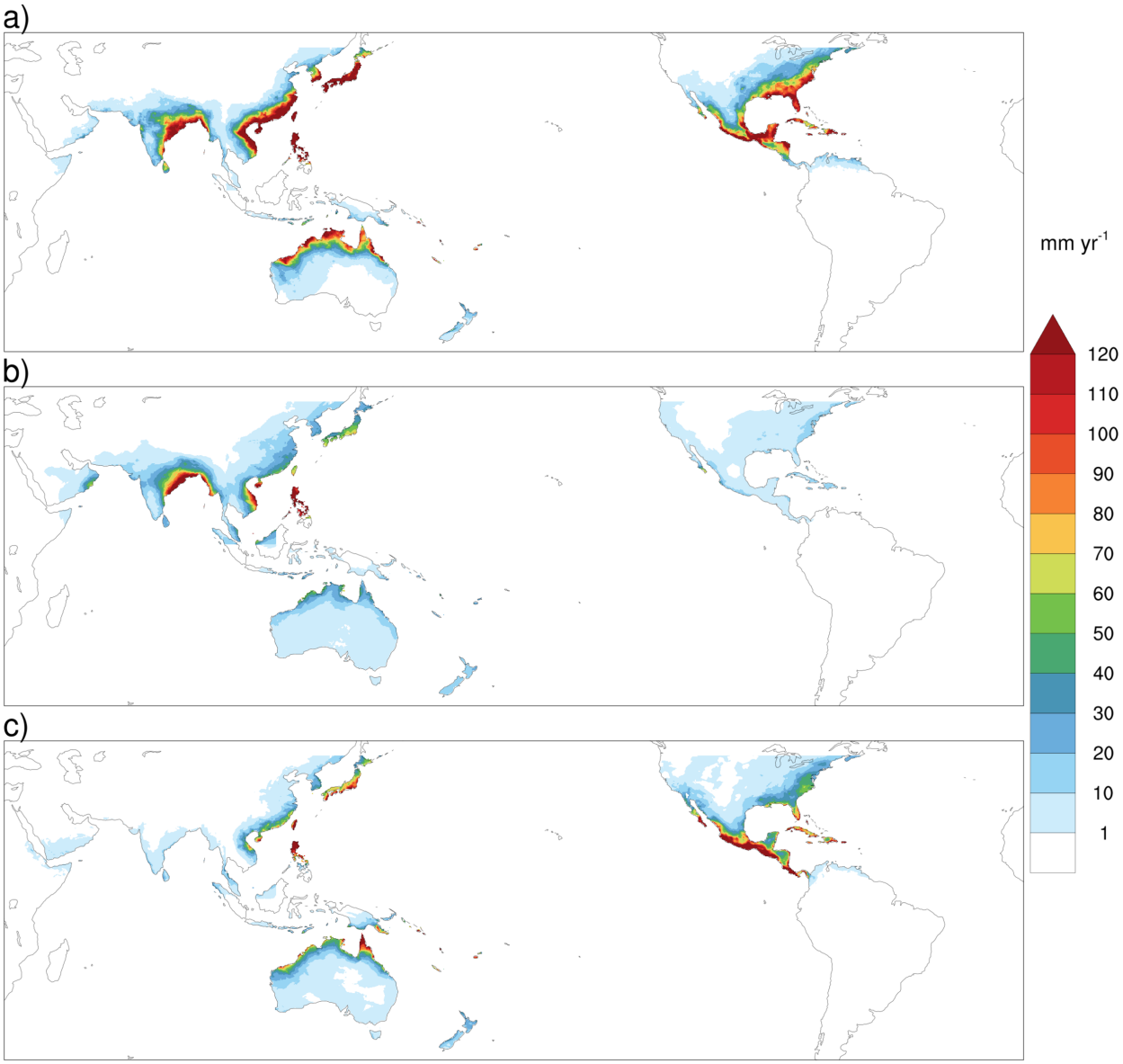

Figure 5. Spatial distribution of the mean annual TC rainfall (mm yr^{-1}) from a) IBTrACS with MSWEP precipitation, b) GCM ensemble mean and c) RegCM ensemble mean.

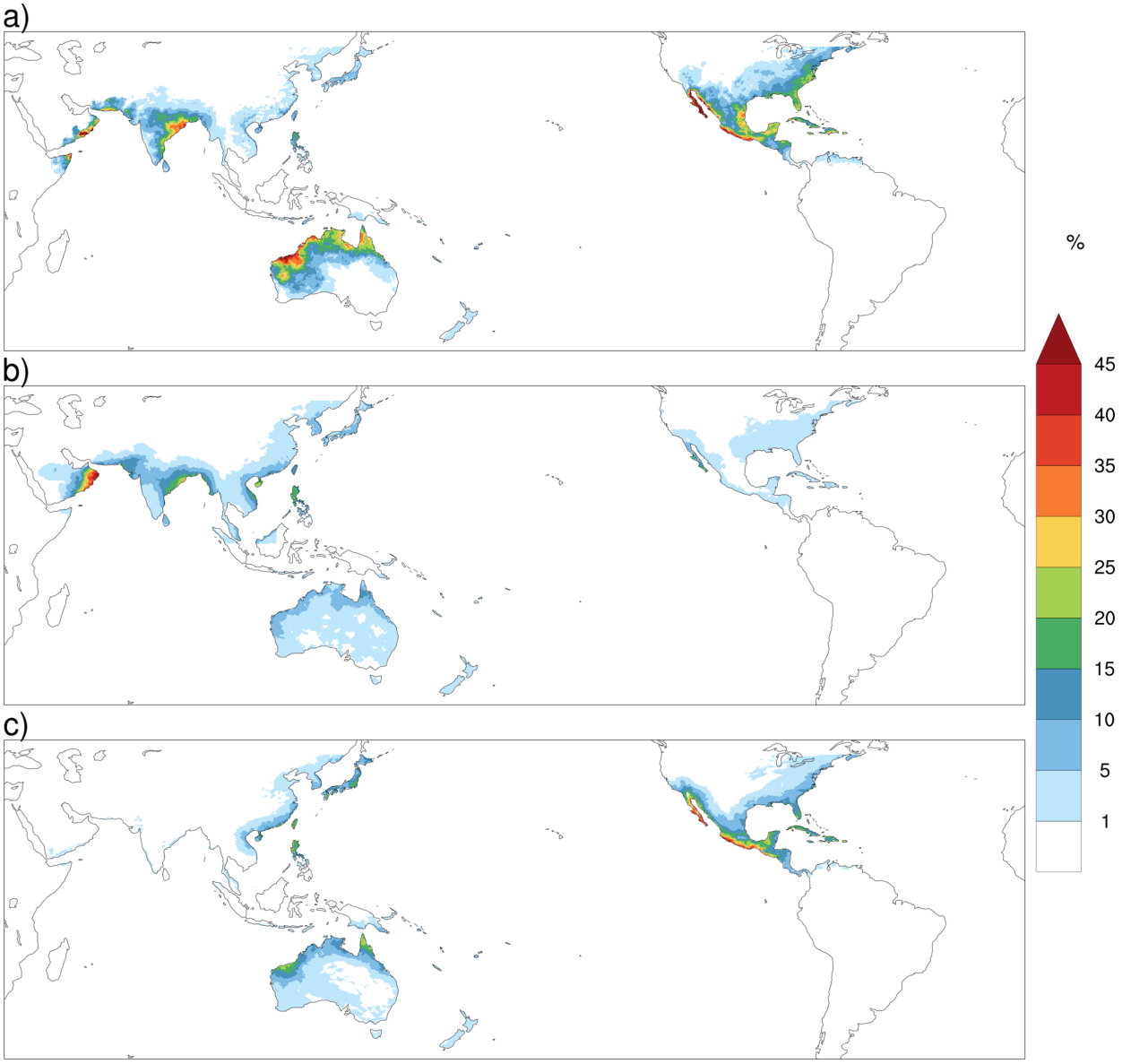

Figure 6. Relative contribution of TCs to extreme rainfall using the POT approach (%, left column) for the (top – bottom) IBTrACS with MSWEP precipitation, GCM ensemble mean and RegCM4 ensemble mean.

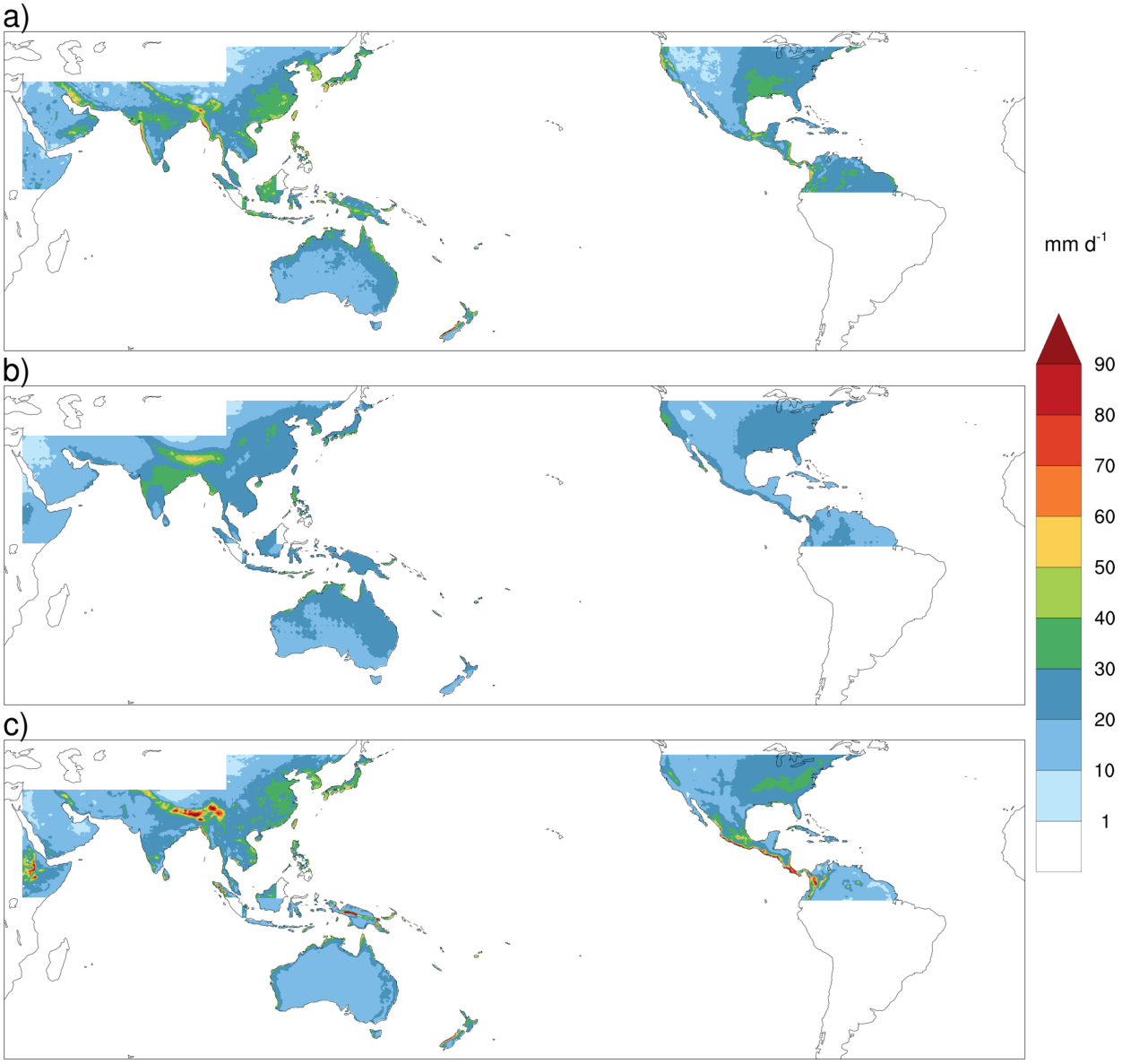

Figure 7. 95th percentile of precipitation (mm d^{-1}) for the (top – bottom) IBTrACS with MSWEP precipitation, GCM ensemble mean and RegCM4 ensemble mean.

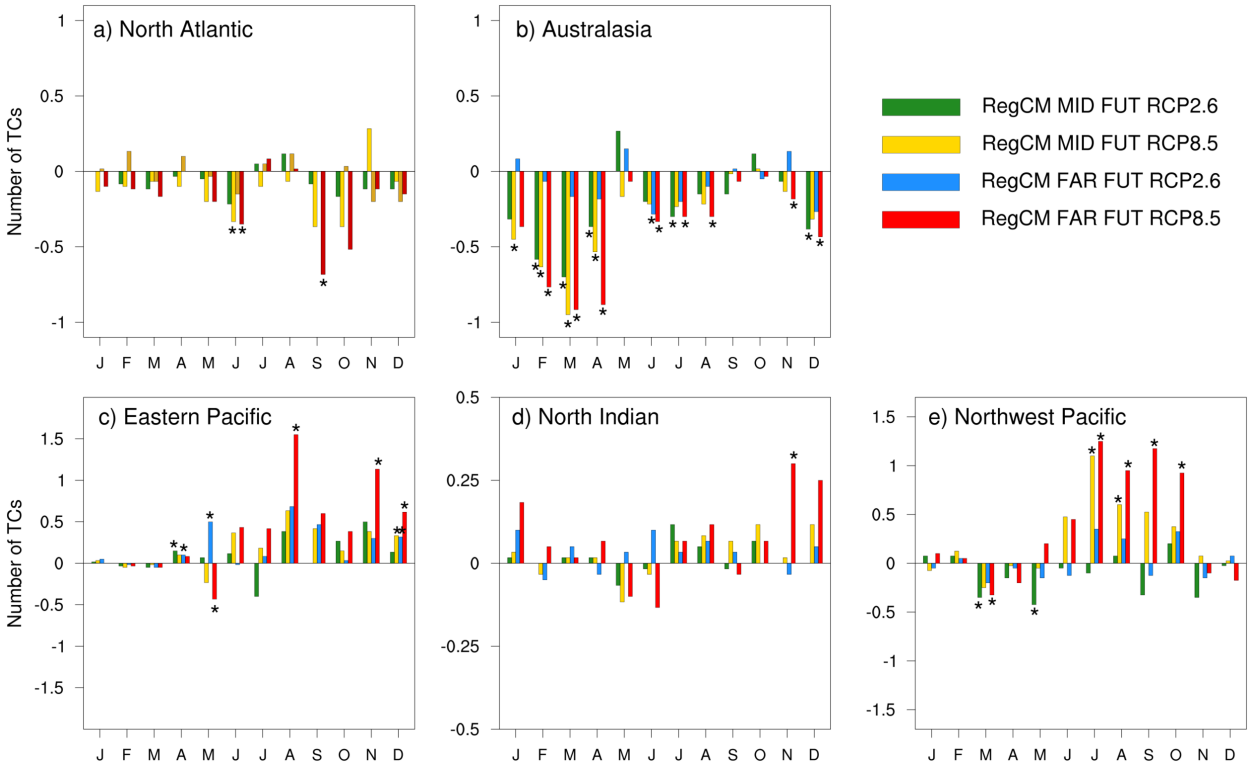

Figure 8. Changes in TC annual cycles for the RegCM4 for the a) North Atlantic, b) Australasia c) the Eastern Pacific, d) the North Indian and e) Northwest Pacific Ocean. Mid-future period refers to 2041–2060 and Far-Future period refers to 2080-2099. Asterisks show where changes are significant to a 95% level of confidence, based on the Wilcoxon rank-sum test.

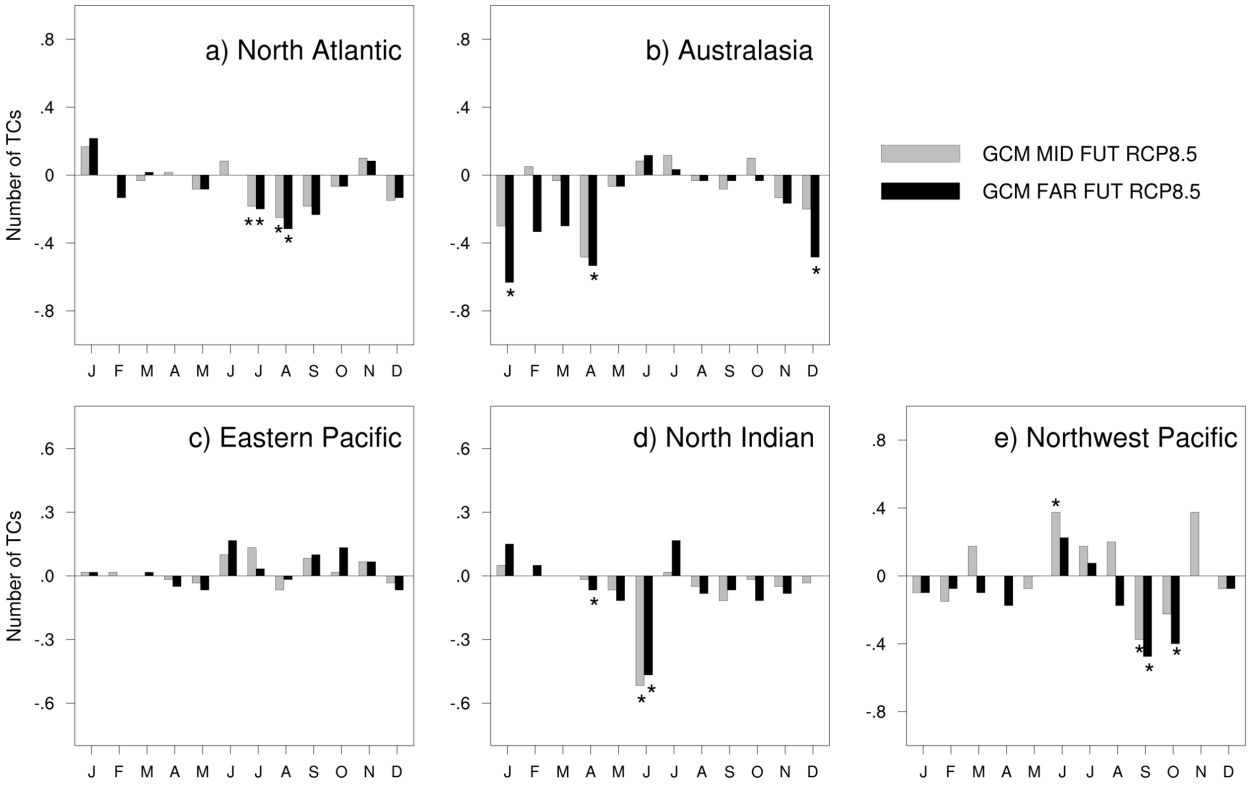

Figure 9. As in Figure 8, but for the GCMs under the RCP8.5 scenario

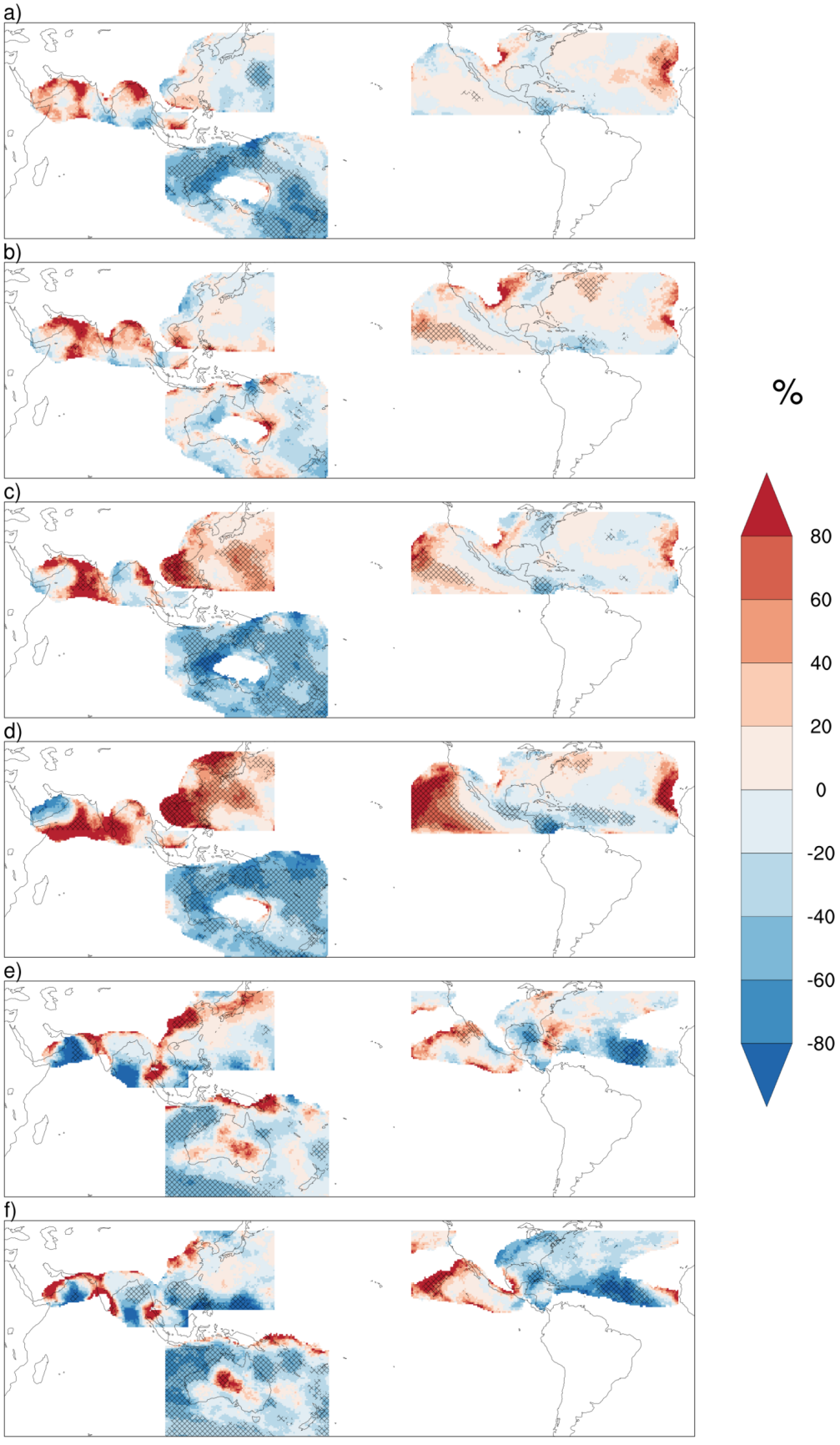
a)
b)
c)
d)
e)
f)
%
80
60
40
20
0
-20
-40
-60
-80

Figure 10. Percent change in TC track density relative to the baseline period for the RegCM ensemble mean under the RCP2.6 scenario for the (a) mid- and (b) late future; under the RCP8.5 scenario for the (c) mid- and (d) late future and for the GCM ensemble (e) mid- and (f) late future. Mid-future period refers to 2041–2060 and Far-Future period refers to 2080-2099. The map show regions with a track density of least 5 days in the historical period. Hatched areas show where changes are significant to a 95% level of confidence, based on the Wilcoxon rank-sum test.

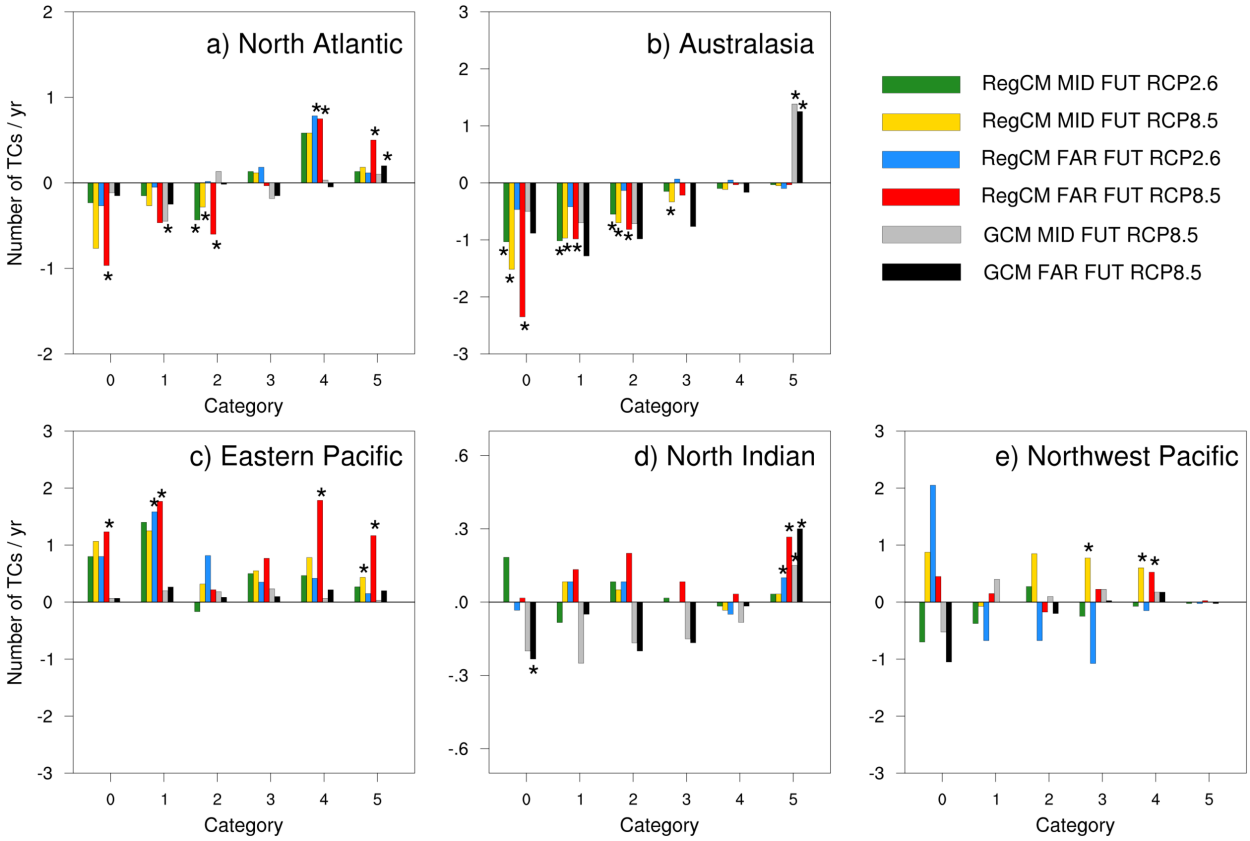

Figure 11. Changes in the annual number of TCs as categorized by the Saffir-Simpson scale for the a) North Atlantic, b) Australasia c) the Eastern Pacific, d) the North Indian and e) Northwest Pacific Ocean. Asterisks show where changes are significant to a 95% level of confidence, based on the Wilcoxon rank-sum test.

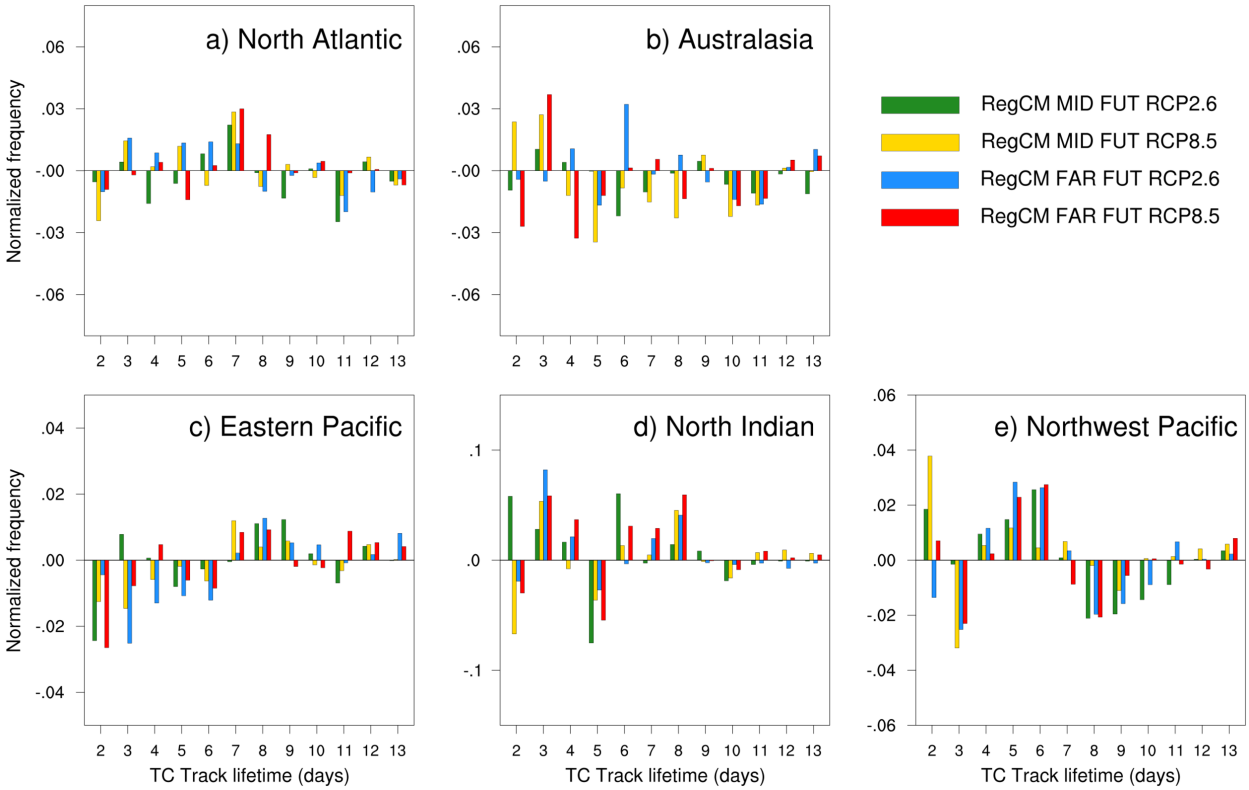

Figure 12. Normalized changes in the life cycle of TCs for the RegCM4 for the a) North Atlantic, b) Australasia, c) the Eastern Pacific, d) the North Indian and e) Northwest Pacific Ocean. Before calculating the differences, the values of life duration were normalized with respect to the total number of TC in each period.

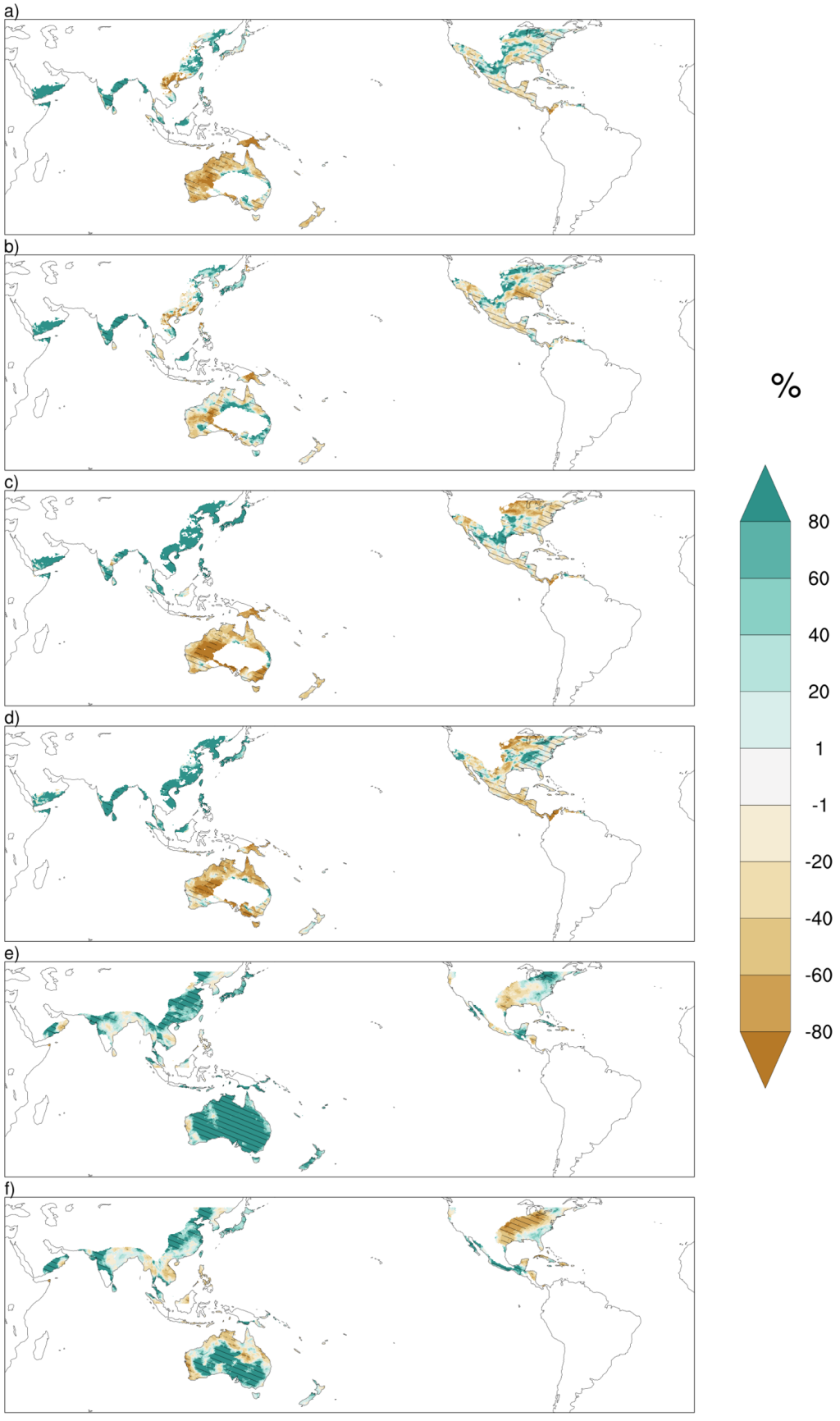
a)
b)
c)
d)
e)
f)
%
80
60
40
20
1
-1
-20
-40
-60
-80

Figure 13. Changes in the total mean annual TC rainfall for the RegCM ensemble mean under the RCP2.6 scenario for the (a) mid- and (b) late future; under the RCP8.5 for the (c) mid- and (d) late future and for the GCM ensemble (e) mid- and (f) late future. The map show regions with precipitation greater than 1 mm/day and with a track density of least 5 days in the historical period. Hatched areas show where changes are significant at a 95% level of confidence, based on the Wilcoxon rank-sum test.

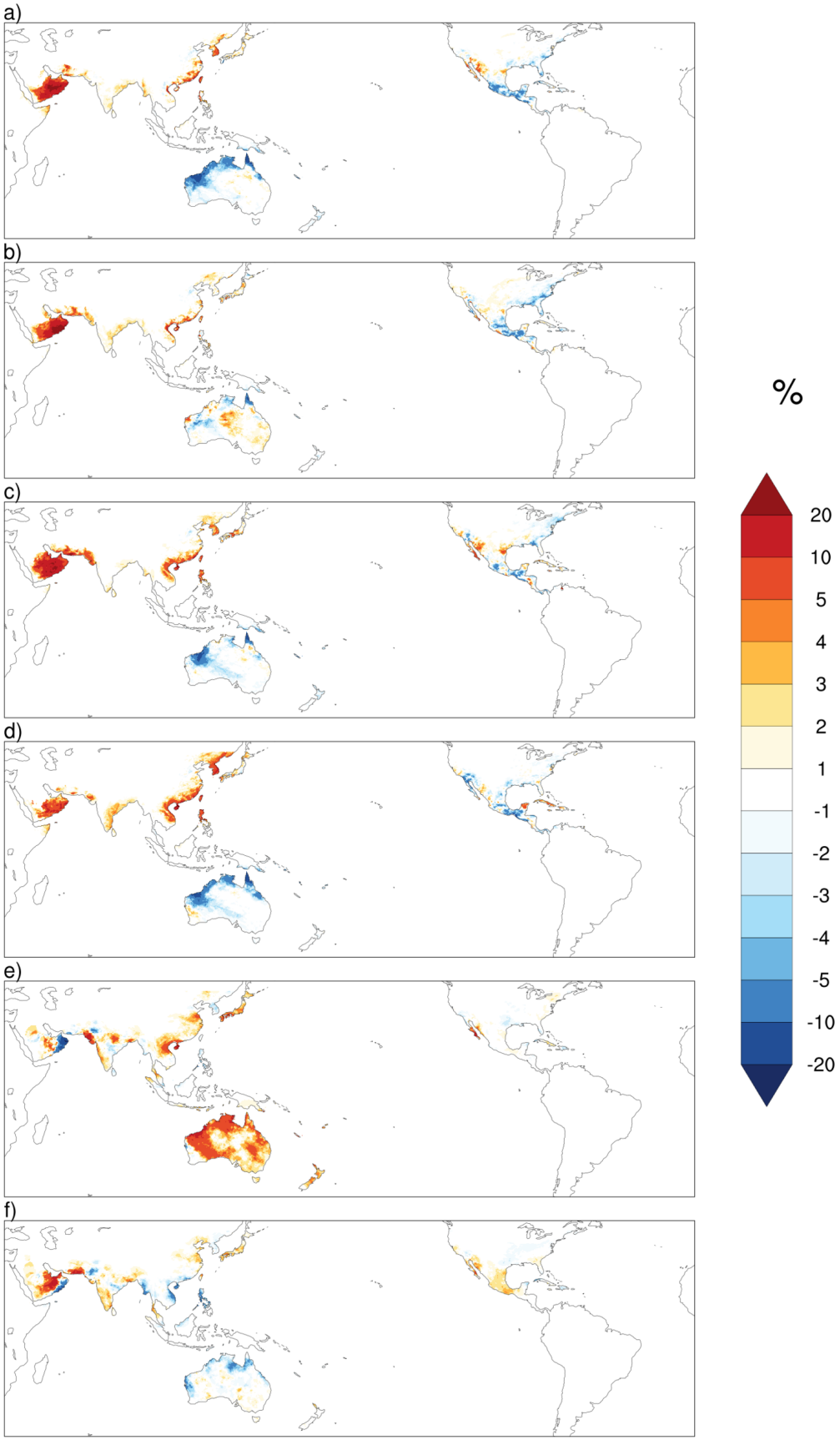
a)
b)
c)
d)
e)
f)
%
20
10
5
4
3
2
1
-1
-2
-3
-4
-5
-10
-20

Figure 14. Changes in contributions of TCs to extreme rainfall using POT approaches for the RegCM ensemble mean under the RCP2.6 scenario for the (a) mid- and (b) late future; under the RCP8.5 for the (c) mid- and (d) late future and for the GCM ensemble (e) mid- and (f) late future.

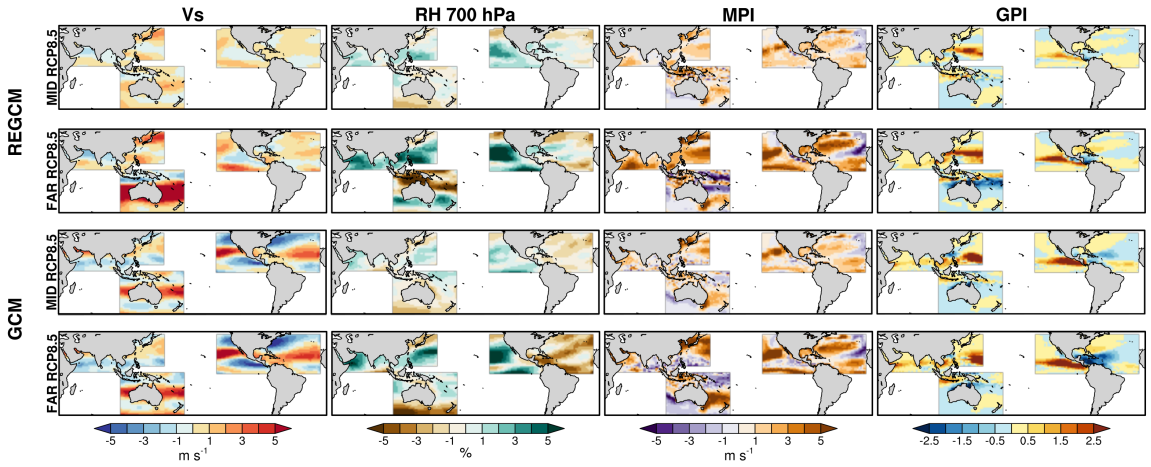

Figure 15. Changes in large-scale environmental parameters associated with hurricane intensity and activity in (left)–(right) vertical wind shear between 850 and 200 hPa (m s^{-1}), 700 hPa relative humidity (%), wind maximum potential intensity (MPI, m s^{-1}), and genesis potential index (GPI), in (top)–(bottom) for the RegCM4 in the RCP8.5 for the mid- and late future and the GCM in the RCP8.5 for the mid- and late future. The mean differences were calculated for the June-November season for the Atlantic, Western and Eastern Pacific basins, the November-March season for the Australasia domain and for the months of May, June, September-December for the North Indian Ocean.

List of Tables

Table 1. Details for models used in the simulations in each domain

Region	Driving GCMs	Physics Scheme	Parametrization	Reference
Australasia	HadGEM2-ES (Collins et al. 2011) MPI-ESM-MR (Zanchettin et al. 2013) NorESM1-M (Zhang et al. 2012)	Boundary Layer	Holtslag	Holtslag, 1990
		Cumulus (Land)	Tiedtke	Tiedtke,1996
		Cumulus (Ocean)	Tiedtke	Kain-Fritsch, 1990, 2004
		Microphysics	SUBEX	Pal et al 2000
		Ocean Flux	Zeng et al	Zeng et al 1998
North Atlantic and Eastern Pacific	HadGEM2-ES MPI-ESM-MR GFDL-ESM2M (Dunne et al. 2012)	Boundary Layer	Holtslag	
		Cumulus (Land)	Emanuel	Emanuel,1991
		Cumulus (Ocean)	Kain-Fritsch	
		Microphysics	SUBEX	
		Ocean Flux	Zeng et al	
North Indian	MPI-ESM-MR NorESM1-M MIROC5 (Watanabe et al. 2010)	Boundary Layer	UW PBL (2)	Bretherton et al. 2004
		Cumulus (Land)	Emanuel	
		Cumulus (Ocean)	Tiedtke	
		Microphysics	SUBEX	
		Ocean Flux	Zeng et al	
Northwest Pacific	MPI-ESM-MR NorESM1-M	Boundary Layer	Holtslag	
		Cumulus (Land)	Emanuel	
		Cumulus (Ocean)	Emanuel	
		Microphysics	SUBEX	
		Ocean Flux	Zeng et al	

Table 2. Correlation coefficients between model and observed TC annual cycle *(R*) and their mean absolute error (MAE).

	North Atlantic		Australasia		Eastern Pacific		North Indian		Northwestern Pacific	
	R	MAE	R	MAE	R	MAE	R	MAE	R	MAE
GCM ensemble	0.81	1.04	0.94	0.35	0.95	0.88	0.44	0.27	0.55	1.28
GCM HadGEM2-ES	0.36	1.10	0.91	0.66	0.86	0.97				
GCM MPI-ESM-MR	0.95	0.84	0.97	0.55	0.99	0.57	0.28	0.35	0.68	1.01
GCM NorESM1-M			0.67	0.38			-0.04	0.32	-0.03	1.62
GCM MIROC5							0.63	0.22		
GCM GFDL-ESM2M	-0.22	1.22			0.28	1.11				
RegCM4 ensemble	0.88	0.6	0.85	0.38	0.94	1.08	0.42	0.23	0.91	0.71
RegCM4 HadGEM2-ES	0.41	1.04	0.84	0.27	0.93	0.72				
RegCM4 MPI-ESM-MR	0.92	1.03	0.92	0.36	0.9	1.03	0.42	0.23	0.86	0.68
RegCM4 NorESM1-M			0.56	0.61			0.04	0.31	0.91	1.06
RegCM4 MIROC5							0.39	0.27		
RegCM4 GFDL-ESM2M	0.89	0.57			0.82	1.63				

Table 3. Correlation coefficients between model and observed life cycle (normalized frequency) of TC *(R*) and their mean absolute error (MAE).

	North Atlantic		Australasia		Eastern Pacific		North Indian		Northwestern Pacific	
	R	MAE	R	MAE	R	MAE	R	MAE	R	MAE
GCM ensemble	0.83	0.025	0.89	0.017	0.63	0.042	0.85	0.020	0.65	0.032
RegCM4 ensemble	0.95	0.017	0.92	0.016	0.75	0.037	0.86	0.028	0.97	0.010

Table 4. Correlation coefficients between model and observed TC rainfall *(R*) and their mean absolute error (MAE, mm).

	North Atlantic		Australasia		Eastern Pacific		North Indian		Northwestern Pacific	
	R	MAE	R	MAE	R	MAE	R	MAE	R	MAE
GCM ensemble	0.81	16.2	0.89	14.4	0.64	6.9	0.92	6.8	0.83	31
RegCM4 ensemble	0.85	11	0.83	10.9	0.86	7.6	0.37	16	0.91	32.5

Table 5. Correlation coefficients between model and observed contribution of TCs to extremes of precipitation *(R*) and their mean absolute error (MAE; %).

	North Atlantic		**Australasia**		**Eastern Pacific**		**North Indian**		**Northwestern Pacific**	
	R	MAE	R	MAE	R	MAE	R	MAE	R	MAE
GCM ens	0.79	3	0.86	6	0.83	2	0.75	3	0.84	1
RegCM ens	0.9	2	0.9	4	0.88	1	0.44	5	0.83	1

Table 6. Tropical cyclone activity (percent change) statistics for RegCM4 ensemble (near or far future vs historical period), over the regions of the Figure 2a.

	North Atlantic				**Australasia**				**Eastern Pacific**				**North Indian**				**Northwestern Pacific**			
Scenario	RCP2.6		RCP8.5		RCP2.6		RCP8.5		RCP2.6		RCP8.5		RCP2.6		RCP8.5		RCP2.6		RCP8.5	
Period	N.F.	F.F.	N.F.	F.F.	N.F.	F.F.	N.F.	F.F.	N.F.	F.F.	N.F.	F.F.	N.F.	F.F.	N.F.	F.F.	N.F.	F.F.	N.F.	F.F.
No. of TC (cat 0-5)	0	5	-3	-6	-30	-10	-38	-45	15	19	21	33	15	13	9	52	-8	-4	21	9
No. of hur (cat 3-5)	25	31	26	35	-22	1	-38	-21	22	16	31	66	22	33	0	255	-18	-65	71	40
TC rainfall (total)	22	6	6	-1	21	19	11	24	26	8	18	0	245	221	255	324	77	75	100	132
Contribution of TCs to extremes of precipitation	17	22	-1	-23	-27	51	-38	-42	11	32	14	-21	456	430	386	431	33	29	82	126

Supplementary materials

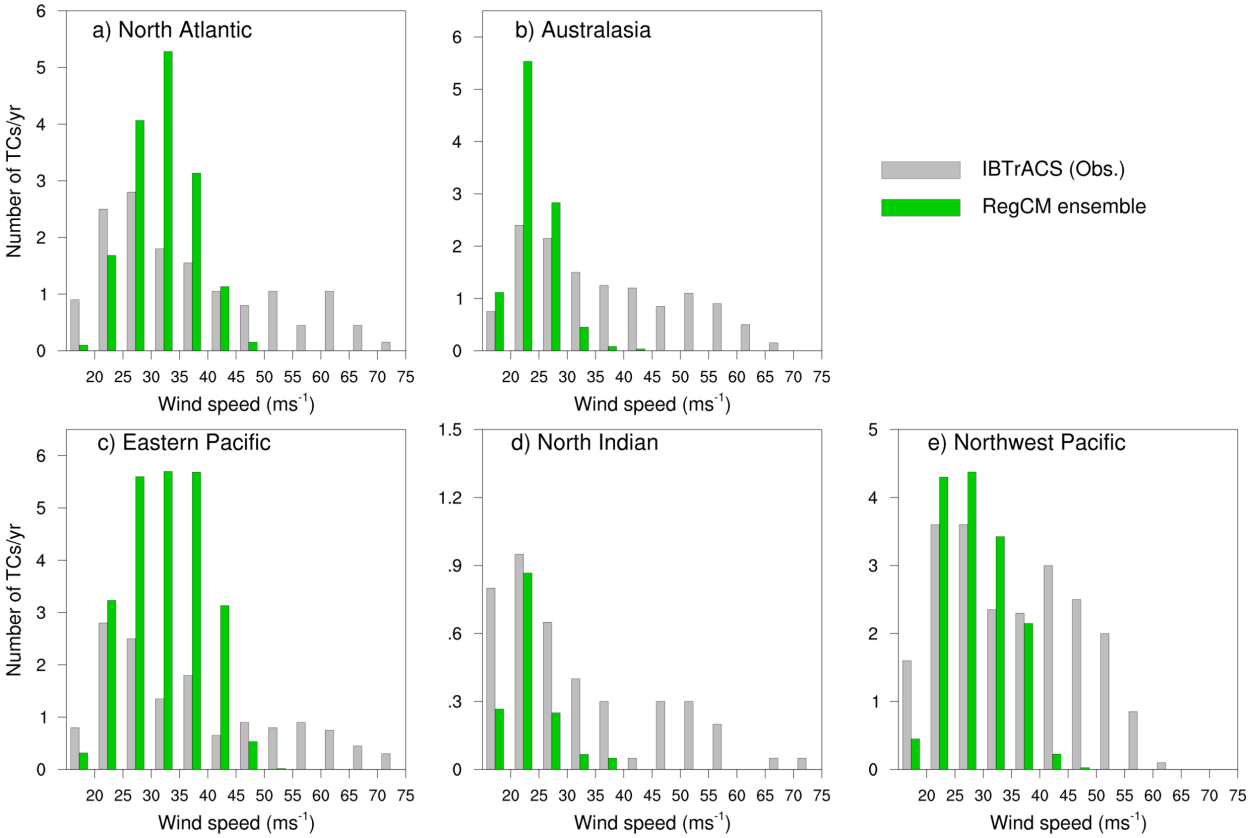

Figure S1. Annual number of TCs categorized by the 10-m wind speed for the a) North Atlantic, b) Australasia, c) the Eastern Pacific, d) the North Indian and e) Northwest Pacific Ocean for 1995-2014.

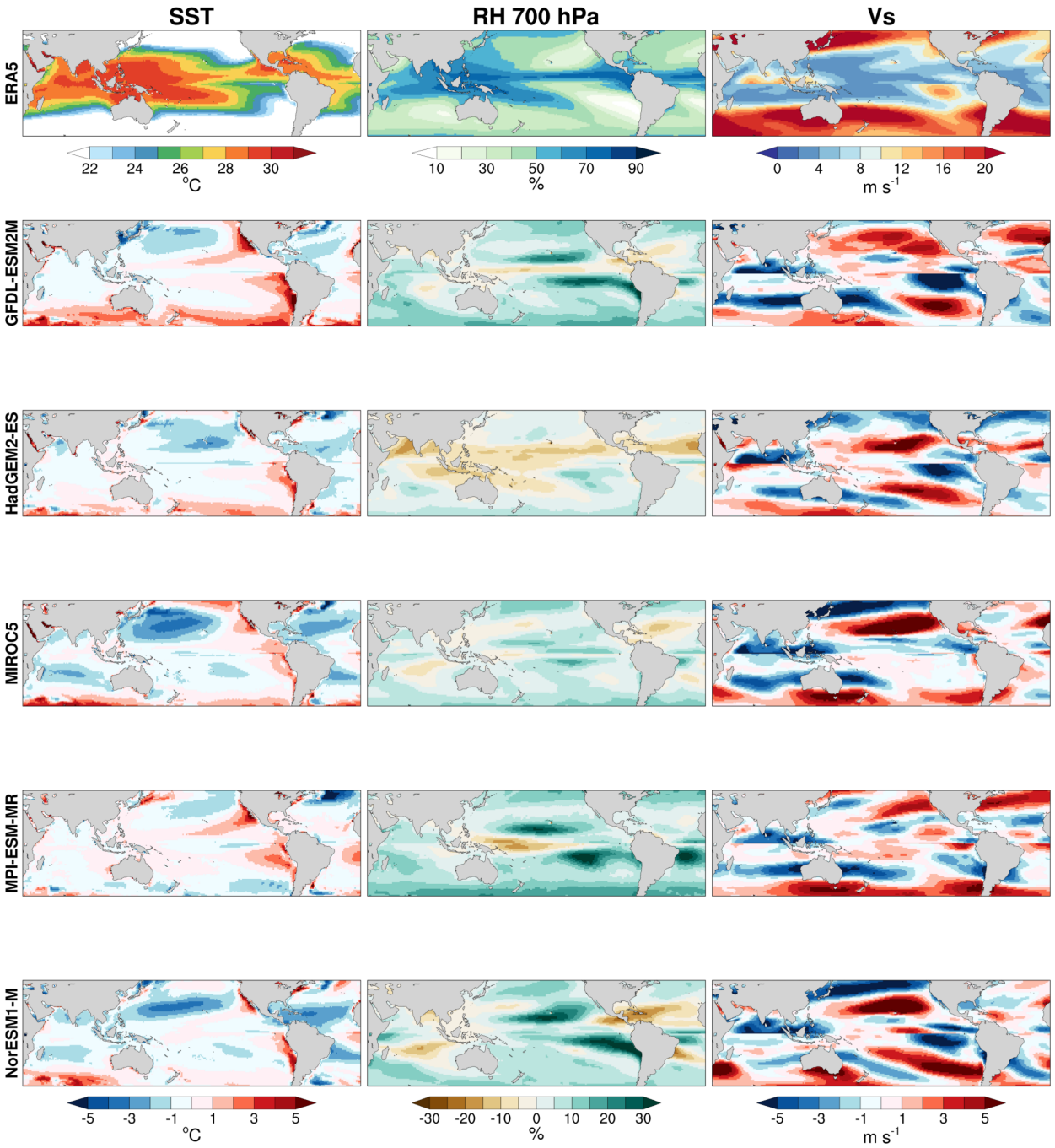

Figure S2. Seasonal climatological fields for the period 1995–2014 in (left)–(right) Sea Surface Temperature (SST, °C), 700 hPa relative humidity (%) and vertical wind shear between 850 and 200 hPa (m s−1), in (top)–(bottom) in the ERA5 reanalysis and the bias for GFDL-ESM2M, HadGEM2-ES, MIROC5, MPI-ESM-MR and NorESM1-M. The Northern (Southern) Hemisphere show the seasonal mean for the May–October (November–April) season.

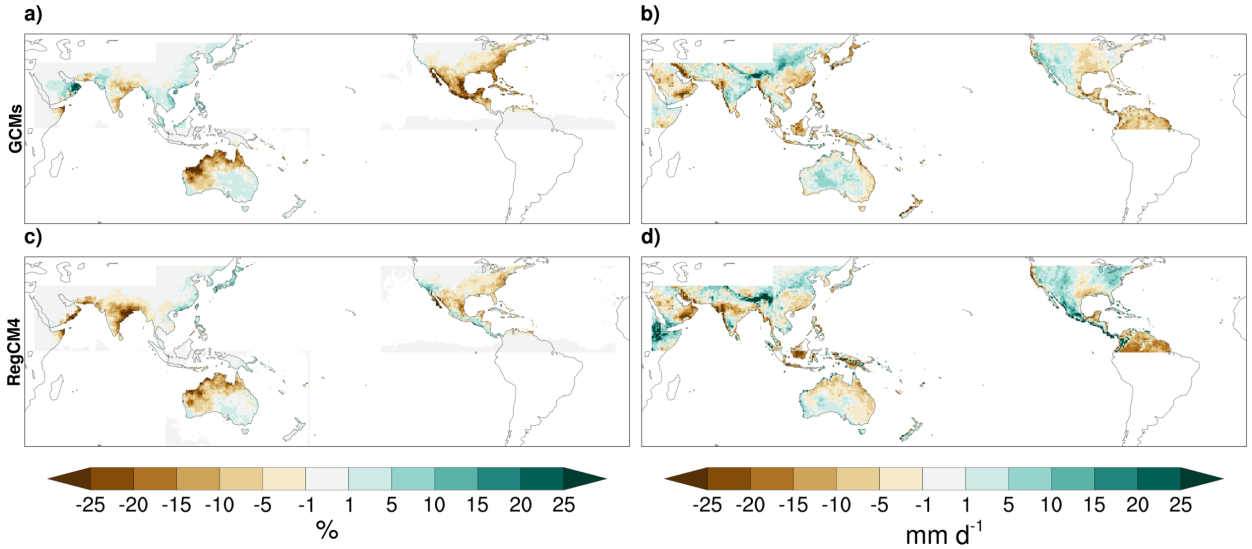

Figure S3. Bias of the relative contribution of TCs to extreme rainfall using the POT approach (%, left column) and 95th percentile of all precipitation (mm d^{-1}, right column) for the (top – bottom) GCM ensemble mean and RegCM4 ensemble mean.

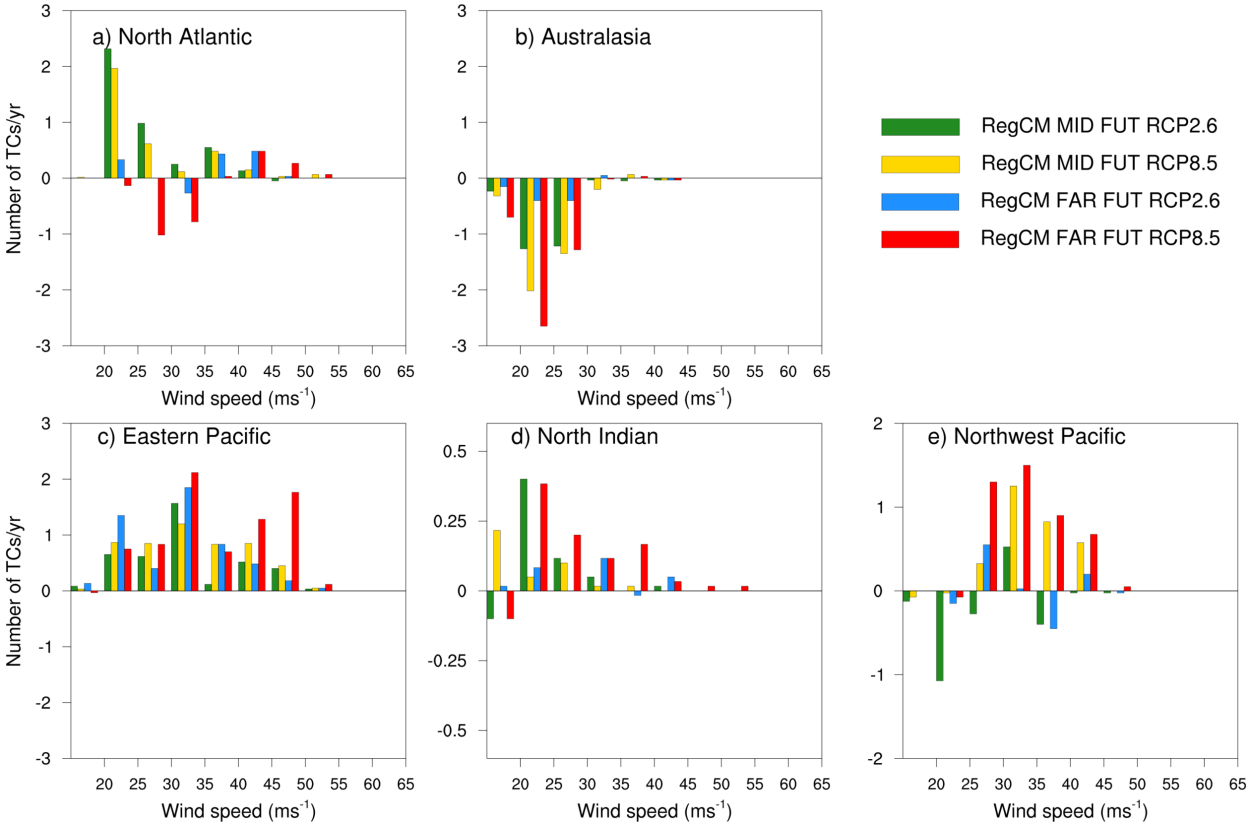

Figure S4. Changes in the annual number of TCs by the 10-m wind speed for the a) North Atlantic, b) Australasia c) the Eastern Pacific, d) the North Indian and e) Northwest Pacific Ocean.

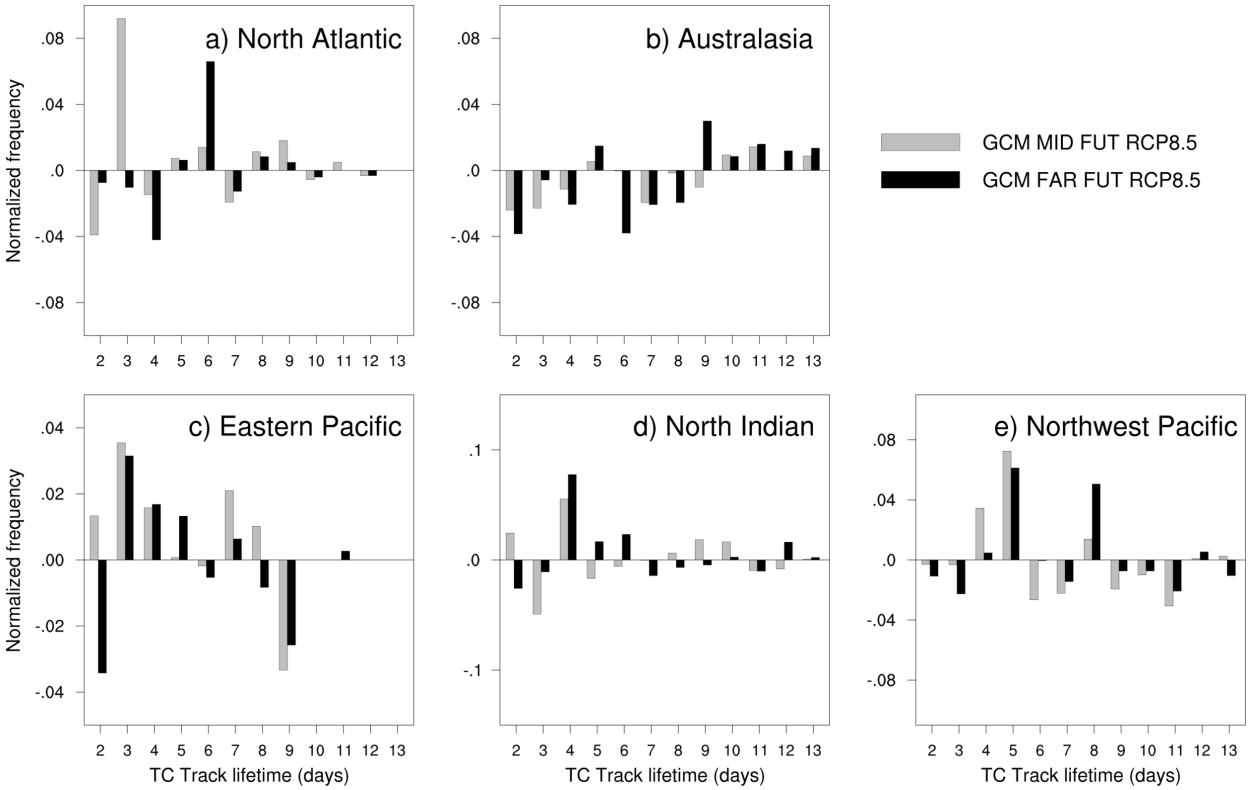

Figure S5. Normalized changes in the life cycle of TCs for the GCMs under the RCP8.5 scenario for the a) North Atlantic, b) Australasia, c) the Eastern Pacific, d) the North Indian and e) Northwest Pacific Ocean. Before calculating the differences, the values of life duration were normalized with respect to the total number of TC in each period.

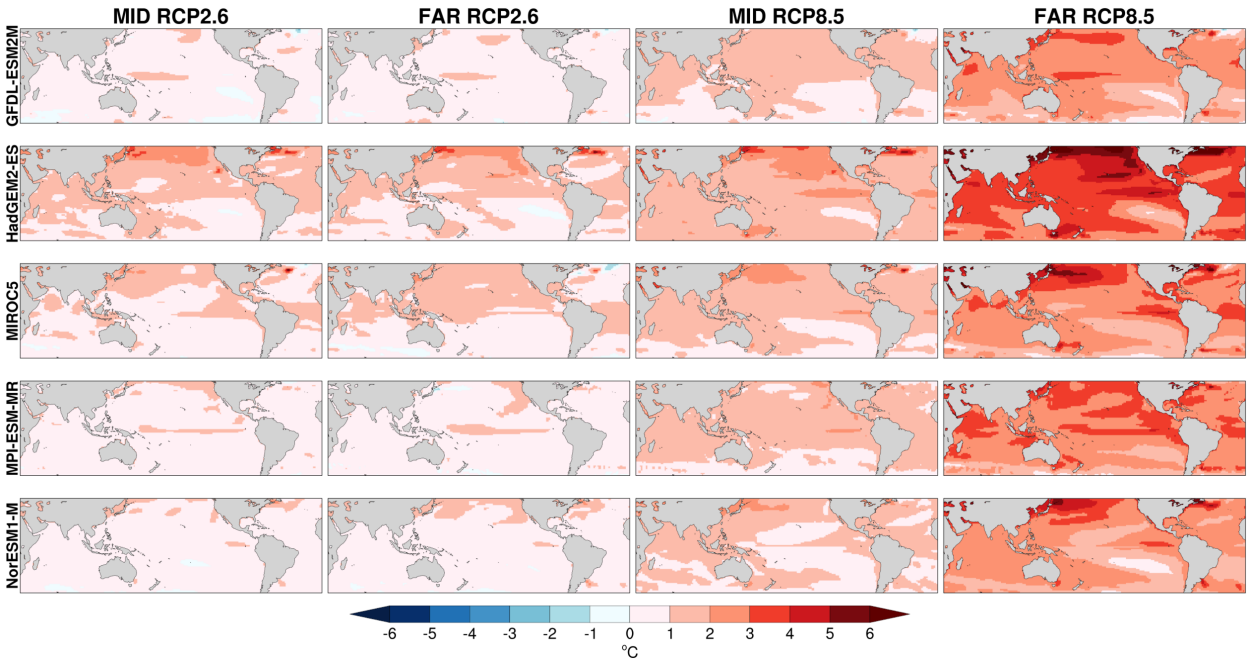

Figure S6. Changes in Sea Surface Temperature (SST, °C) for CMIP5 models in (left)–(right) in the RCP2.6 scenario for the mid- and late future, and under the RCP8.5 for the mid- and late future, in (top)–(bottom) GFDL-ESM2M, HadGEM2-ES, MIROC5, MPI-ESM-MR and NorESM1-M. The Northern (Southern) Hemisphere shows the seasonal mean for the May–October (November–April) season.

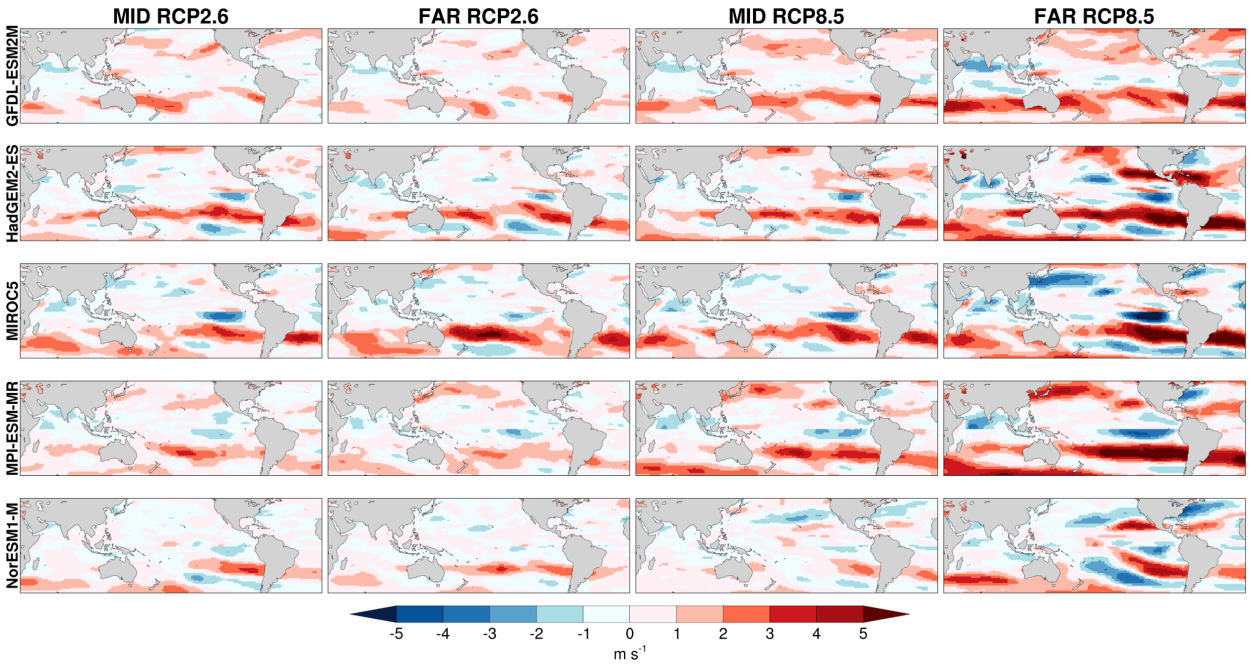

Figure S7. Changes in vertical wind shear between 850 and 200 hPa (m s^{-1}) for CMIP5 models in (left)–(right) in the RCP2.6 scenario for the mid- and late future, and under the RCP8.5 for the mid- and late future, in (top)–(bottom) GFDL-ESM2M, HadGEM2-ES, MIROC5, MPI-ESM-MR and NorESM1-M. The Northern (Southern) Hemisphere shows the seasonal mean for the May–October (November–April) season.